NTNU
Norwegian University of
Science and Technology

Modeling and control of a calcination furnace

Øyvind Wilson

Master of Science in Cybernetics and Robotics
Submission date: June 2017
Supervisor: Morten Hovd, ITK
Co-supervisor: Stein Wasbø, Cybernetica

Norwegian University of Science and Technology
Department of Engineering Cybernetics

Summary

Calcined anthracite is the primary material used in Søderberg electrode paste, prebaked carbon electrodes, aluminium cathodes, and a variety of other carbon products used in the metallurgical industries.

In electrical calcination of anthracite current is passed through the raw material. This heat treats the anthracite, which gets rid of volatile matter and water, and graphitizes the anthracite. The graphitization lower the anthracite's electrical resistivity. The object of the process is to get calcined anthracite with resistivity inside a given range.

Elkem's electric calciner is the process examined in this work. It is in a large degree controlled manually, and the present control leads to inconsistent product results. The main motivation for this work is to develop a controller that yields automatic and consistent control of the process. In this work, the first steps towards this goal is started.

A first principle mathematical model is developed for the process. Mass and energy balances are used, as well as a description of the resistivity change. The electrical properties of the process is also looked upon and modelled. Further the model is simulated and compared to real operational data from Elkem's calcination furnace to check its validity.

Current and voltage is both used as input to see which gives the best result. It is seen that current as an input undoubtedly yields much better results than when voltage is used as input. The introduction of thermal runaway in the model is speculated to be the reason.

The effect of the effective activation energy on the resistivity curve is examined. No general rule for its behaviour is found.

The finished model gives satisfactory matches with all the measured electrical properties except for the resistivity. Since there isn't any observable correlation between the inputs and the measured resistivity, or any correlation between the measure resistance and resistivity, it is suspected that the resistivity measurements are not trustworthy. These measurements is dismissed. For the continuation of this work, the model is assumed verified based on the other measurements (primarily the furnace resistance).

A formulation for an NMPC controller is suggested. Two cases are simulated using the model both as a model for the plant and the model used in the controller. The first case concerns changes of the resistivity set point without any model deviations or disturbances. The second case concerns a change in the raw material's moisture modelled as a disturbance. This case is examined both with and without feed-forward.

The controller works well when there are no disturbances or model deviations. When the change in the raw material's moisture is introduced as a disturbance, the controller is no longer able to reach the desired set point. Using feed-forward fixes this problem, and yields smooth and efficient control to the set point.

Sammendrag

Kalsinert antrasitt er hovedmaterialet brukt i Søderberg elektrodepasta, forbakte karbonelektroder, aluminiumskatoder, og i en rekke andre karbonprodukter brukt i de metallurgisk industriene.

I elektrisk kalsinering av antrasitt sendes strøm gjennom råmaterialene. Dette varmebehandler antrasitten, noe som fjerner flyktige stoffer og vann, samt grafittiserer antrasitten. Grafittiseringen minsker antrasittens elektriske resistivitet. Målet for prosessen er å få kalsinert antrasitt med resistivitet innenfor et gitt område.

Elkems elektriske kalsineringsovn er prosessen som blir undersøkt i dette arbeidet. Den er i stor grad styrt manuelt, og den nåværende styringen fører til ujevn prosesskvalitet. Hovedmotivasjonen for dette arbeidet er å utvikle en regulator som gir automatisk og jevn styring av prosessen. I dette arbeidet er de første stegene mot dette målet tatt.

En matematisk modell er utviklet basert på fysikalske grunnprinsipp. Masse- og energibalanser er brukt, i tillegg til beskrivelser av resistivitetendring. De elektriske egenskapene til prosessen er også undersøkt og modellert. Videre så er modellen simulert og sammenlignet med ekte operasjonsdata fra Elkems kalsineringsovn for å sjekke modellens gyldighet.

Både strøm og spenning er brukt som pådrag, og sammenlignet for å se hva som gir best resultater. Det er observert at strøm utvilsomt gir bedre resultater når brukt som pådrag, enn det spenning gir. Det er spekulert om innføring av termisk rømling i modellen kan være grunnen.

Effekten av den effektive aktiveringsenergien er undersøkt. Ingen generell regel for dens oppførsel er funnet.

Den ferdige modellen passer godt med målingene for alle elektriske egenskaper sett bort i fra resistiviteten. Siden det ikke kan sees noen direkte sammenheng mellom pådragene og den målte resistiviteten, eller noen sammenheng mellom motstandsmålingene og resistvitetsmålingene er det en mistanke om at resistivitetsmålingen ikke er særlig pålitelige. Disse målingene er derfor sett bort ifra. For fortsettelsen av dette arbeidet er det antatt at modellen er god nok på grunn lag av de andre målingene. Det er særlig lagt vekt på motstandsmålingene.

En formulering for en NMPC-regulator er foreslått. To problem er simulert. I begge tilfellene er modellen brukt både som reguleringsmodell og som anleggsmodell. Det første problemet omhandler regulering til settpunkt uten modellavvik eller forstyrrelser. I det andre problemet er endringer i råmaterialets fuktighetsinnhold modellert som en forstyrrelse. Dette problemet er undersøkt både med og uten ”feed-forward”.

Regulatoren fungerer fint når det ikke er forstyrrelser eller modellavvik. Når endringer i fuktighetsinnholdet er innført som en forstyrrelse, klarer ikke regulatoren lenger å nå settpunktet. Når ”feed-forward” blir brukt løses imidlertid dette problemet, og man får effektiv og glatt regulering til settpunktet.

Preface

This master's thesis is written in the spring of 2017. It is the final part of the study program Cybernetics and Robotics at the Norwegian University of Science and Technology, leading to a Master of Science degree. The thesis has been written at the Department of Engineering Cybernetics, in close collaboration with the company Cybernetica AS, which proposed the thesis.

First of all I want to thank all the employees at Cybernetica for making me feel welcome at their office, and for all help and support. I appreciate that time and resources has been used to help me in my work. A special thanks goes to my co-supervisor Stein Wasbø, who has been my biggest support, and who always has been ready to help in any way possible.

Next I want to thank Elkem for trusting me, and granting me access to sensitive and confidential information. I'm very grateful for the opportunity to come down to Kristiansand and actually see the plant for myself; this was of great value for my work with this thesis. I particularly want to thank my contacts in Elkem, Åslaug Grøvlen and Jesse White, which has answered many question about the process.

At last I want to thank my supervisor Morten Hovd for asking critical questions, and giving me good feedback.

Table of Contents

List of Figures

List of Tables

List of Symbols

Roman letters:

A	Cross section area
$A_{i,j}$	Cross section are between control volume i and j
$A_{i,w}$	Cross section area between control volume and wall
A_p	Cross section area of anthracite particle
$A_{p,tot}$	total cross section area of all the anthracite particles
A_ν	Cross section area of void
a	Unit cell dimension within graphite layers
b	Electrical conductivity constant
$C_{p,i}$	Heat capacity in control volume i
c	Unit cell height of graphite
d	Spacing between graphite layers
d_{002}	Interlayer spacing in crystallites
E	Activation energy
e	Specific energy
f_i	Conversion factor from mass to resistivity
g	Acceleration of gravity
g	Degree of graphitization
g_0	The complement of the degree of graphitization
H	Chemical enthalpy
ΔH_R	Reaction enthalpy from graphitization
ΔH_{R_γ}	Enthalpy from driving off the volatiles
$\Delta H_{R_{\mathrm{H_2O}}}$	Enthalpy from vaporizing water
h	Convection heat transfer coefficient
h_A	Height of all anthracite in control volume
h_p	Height of anthracite particle
h_{shell}	Convection coefficient between steel shell and air
h_{tot}	Total height of control volume
$h_{\mathrm{tot},\nu}$	Height of all void in control volume
h_{wall}	Convection coefficient between anthracite and wall
h_ν	Height of void
I_i	Current in control volume i
i	Control volume
j	Control volume
k	Thermal conductivity
k_b	Thermal conductivity of insulation bricks
k_i	Thermal conductivity of control volume i
k_l	Thermal conductivity of refractory lining

k_s	Thermal conductivity of steel shell
k_ρ	Resistivity reaction rate constant
L	Length
L_a	Stack width in crystallites
L_b	Length of insulation bricks in x-direction
L_c	Stack height in crystallites
L_l	Length of refractory lining in x-direction
L_s	Length of steel shell in x-direction
$l_{i,j}$	Length from the middle of i to the interface between i and j
m_i	Mass in control volume i
N	Prediction horizon
N_L	Number of layers
N_p	Number of particles
n	Graphitization constant
$n_{r,i}$	Number of reactions in control volume i
nu	Input vector dimension
nx	State vector dimension
nz	Output vector dimension
$\boldsymbol{P}$	Slack variable penalty matrix
$\mathbf{p}$	Slack variable penalty vector
p	Pressure
$P_{c,i}$	Heating power from volatile combustion to control volume i
$P_{el,i}$	Heating power from ohmic heating to control volume i
Q	Effective activation energy
Q	Heat transfer
$\boldsymbol{Q}$	Output penalty matrix
q_c	Conduction heat rate
$q_{c'}$	Convection heat rate
q_r	Radiation heat rate
$Q_{c,i,j}$	Conduction heat from control volume i to j
$Q_{i,el}$	Heat from control volume i to the electrode
$Q_{i,top}$	Heat from control volume i over the top
$Q_{i,j}$	Heat from control volume i to control volume j
$Q_{i,0}$	Heat from control volume i out through the wall
$Q_{r,i,j}$	Radiation heat from control volume i to j
R	Universal gas constant
r	Reaction rate
$\boldsymbol{R}$	Input penalty matrix
R_A	Resistance of anthracite particle
R_{eq}	The furnace's equivalent resistance
R_i	Resistance in control volume i
R_L	Resistance of layer
R_{loss}	Resistance for rest of secondary circuit
R_{tot}	Total resistance
R_ν	Resistivity of void space

r_p	Particle radius
$\boldsymbol{S}$	Input change penalty matrix
s_i	Resistivity reaction rate in control volume i
T	Temperature
T_i	Temperature in control volume i
$T_{i,j}$	Temperature on the interface between control volume i and j
T_{wall}	Temperature at the inner edge of the wall
$\mathbf{u}$	Input vector
$\mathbf{\Delta u}$	Input change vector
V	Volume of control volume
$\mathbf{v}$	Velocity vector
V_{furn}	Furnace voltage
V_i	Voltage in control volume i
V_p	Primary voltage
V_s	Secondary voltage
W	Work done to the surroundings
W_s	Work excluding pressure work
$w_{in,i}$	Mass flow in to control volume i
$w_{out,i}$	Mass flow out from control volume i
$\mathbf{x}$	State vector
$X_{\gamma,i}$	Weight fraction of volatiles driven off in control volume i
$X_{\mathrm{H_2O},i}$	Weight fraction of water vaporized in control volume i
y	Process measurements
$\hat{y}$	Modelled measurements
z	Vertical coordinate
$\mathbf{z}$	Output vector

Greek letters:

α	Rate of graphitization
α_0	Graphitization constant
β	Particle stacking parameter
ϵ	Emissivity
ε	Slack variable
θ	Subset of parameters
κ	Electrical conductivity
ν	Void fraction
ν_p	Effective void fraction for resistance
ρ	Electrical resistivity
ρ_A	Electrical resistivity of anthracite particle
ρ_d	Denisty
ρ_ν	Electrical resistivity of void
$\rho_s(T, \text{type})$	Steady state resistivity
τ	Time
σ	Stefan-Boltzmann constant

Abbreviations

CV	=	Controlled Variable
DAE	=	Differential-Algebraic Equation
DCS	=	Distributed Control System
DOG	=	Degree Of Graphtization
FAT	=	Factory Acceptance Tests
ECA	=	Electrically Calcined Anthracite
GCA	=	Gas Calcined Anthracite
GUI	=	Graphical User Interface
MIMO	=	Multiple Input, Multiple Output
MMI	=	Man-Machine Interface
MPC	=	Model Predictive Control
MV	=	Manipulated Variable
NMPC	=	Nonlinear Model Predictive Control
OPC	=	Open Platform Communication

Chapter 1

Introduction

Calcined anthracite has been the primary material used in aluminum smelting cell cathodes for decades (Belitskus, 1977). Petroleum coke is the material that traditionally has been used in making carbon anodes for the aluminium process. However, Yao-jian et al. (2009) showed that carbon anodes that in part consist of calcined anthracite, are superior to anodes that are completely made up of petroleum coke. Calcined anthracite is also used in Søderberg electrode paste, prebaked carbon electrodes, and a variety of other carbon products used in the metallurgical industries.

Through the calcination process it is desirable to obtain calcined anthracite with certain properties. These properties differ depending on what product the calcined anthracite should be used in. It is desirable to develop a mathematical model describing this process. This model will in turn be used in a model based control scheme, which hopefully will lead to better control of the process. The model might also help in understanding the process better.

A specialization project in the fall 2016 preceded this work. In this project, a first draft of a mathematical model was developed and presented in a report, see Wilson (2016). In this work the model developed in the specialization project will be improved. Further a model based control scheme will be proposed.

1.1 Report structure

Chapter 1 gives an introduction to this work. This includes a presentation of industry partners, description of the process, motivation for the work, and challenges related to the specific process.

Chapter 2 gives an brief overview of the basic theory needed for this work. This consist of carbon structure and properties, mass and energy balances, heat transfer and model predictive control.

Chapter 3 introduces the software used in this work, focusing on Cybernetica's tools. These tools are Cybernetica ModelFit, Cybernetica RealSim and Cybernetica CENIT.

Chapter 4 concerns the model and how it is developed. The model is developed using mass balances, resistivity changes, and energy balances. The chapter also contains the electrical model, a function for the bulk resistivity is derived, the heat transfer equations are given, as well as a description of the parameter estimation methods.

In chapter 5 the validity of the model is examined. Voltage and current is compared as input. The effect of the activation energy is looked upon. At last simulation results and discussions for the model is given.

Chapter 6 gives the controller formulation. Two control cases are described.

Chapter 7 present the simulation results of the control cases with discussion.

Chapter 8 gives the conclusion to this work. Suggestions for further works can also be found here.

1.2 Industry partners

1.2.1 Cybernetica

This work has been written in collaboration with Cybernetica. Cybernetica is a small company located in Trondheim, Norway. They specialize in tailor made model based control systems for the process industry. Their main product is software for nonlinear model predictive control (NMPC) called Cybernetica CENIT (Cybernetica, 2017).

1.2.2 Elkem

The process to be modelled is Elkem's electric calcinator (see patent Johansen and Vatland, 2000). Elkem is a company started in Norway in 1904. Now they have over 40 plants and sales offices around the world. They are one of the world's leading companies in production of silicon materials, foundry products and carbon.

Elkem is divided into four business areas: Elkem Silicon Materials, Bluestar Silicones International, Elkem Foundry Products and Elkem Carbon. Elkem Carbon is the division that handles the calcination process. They have provided process data from normal operation of their electric calcinator such that the model can be compared to normal operation.

1.3 Problem description

Cybernetica proposed the following problem:

Cybernetica has a close relationship with Elkem. Elkem Carbon delivers carbon products to a number of metal producers all over the world from their production sites in Norway and Brazil, among other places. A key process in their production is calcination furnaces, where anthracite and other carbon based raw materials get heat treated. The purpose of this heat treatment is to produce carbon with the right electrical properties. The finished product is typically used as material for electrodes in various smelting processes.

It is desirable to improve operation of these calcination furnaces through better control of both chemical composition and electrical properties. To achieve this, a model describing the mass and energy balance has to be developed. The process is a continues process

where raw material gets fed into the furnace and current is introduce through a top electrode, then goes through the carbon material in the furnace, before going through a bottom electrode.The developed model should be validated against operational data, and an optimization control should be proposed. The task will be completed in cooperation with Elkem Carbon in Kristiansand.

1.4 Description of the electric calcination process

Electrical calcination of carbon is a process where carbon-based raw materials such as coke or coal gets heat treated by passing current through it. There are two main reasons for doing this: to get rid of volatile matter and water, and to lower the electrical resistivity (Perron et al., 1996; Lakomskii et al., 2011; Budd et al., 1995; Gasik et al., 2010). The volatiles gets driven off down through the furnace (Elkem Carbon, 2017). The volatile matter is only partially burned in the furnace, before the combustion is completed in a chimney above the furnace (Perron et al., 1996).

The carbon materials undergo structural changes when heated to high temperatures, producing some graphite (Budd et al., 1995). This phenomenon is called graphitization, and is what changes the material's resistivity. Another structural change is shrinkage, which is described in detail in Wallouch and Fair (1980).

Elkem's calcination process is done in a vertical cylindrical furnace filled with carbon material. An example of such a furnace can be seen in Figure 1.1. The electrical resistivity decreases during calcination, which affects the current paths in the furnace (Perron et al., 1996). According to King et al. (1990) a simple model for the electrical resistivity is that it is a function of the maximum temperature that the material has experienced. The resistivity does not go back up again when the carbon is cooled, meaning that the process is not reversible. Elkem Carbon (2017) says that the specific power that the carbon experience determines the resistivity. It is a well known fact that the carbon in the middle of the furnace will be better calcined than the carbon at the sides. This because it is much hotter in the middle.

There are two inputs for Elkem's furnace:

- Power provided the furnace.
- Discharge rate.

The discharge rate is by which rate the mass of the carbon material is discharged from the furnace. The furnace is designed in such a way that it is always filled with carbon material. There are controllers on the inputs.

1.5 Motivation

Elkem has decades of experience making electrically calcined anthracite (ECA). Despite this the calcination process is to a large degree controlled manually. As previously stated there are controllers for the inputs: power and discharge rate. There is however, no control of the electrical resistivity.

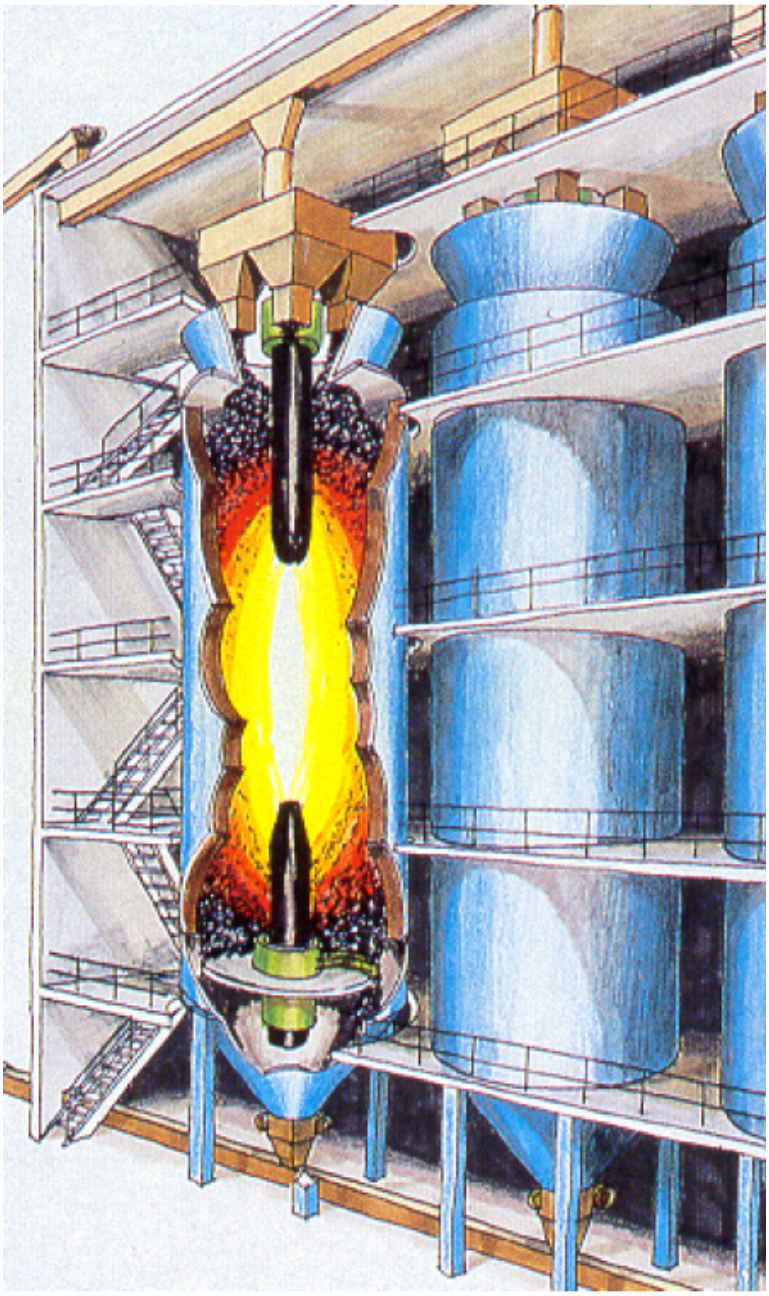

Figure 1.1: Elkem's electrical calcinator. From Elkem Carbon (2017).

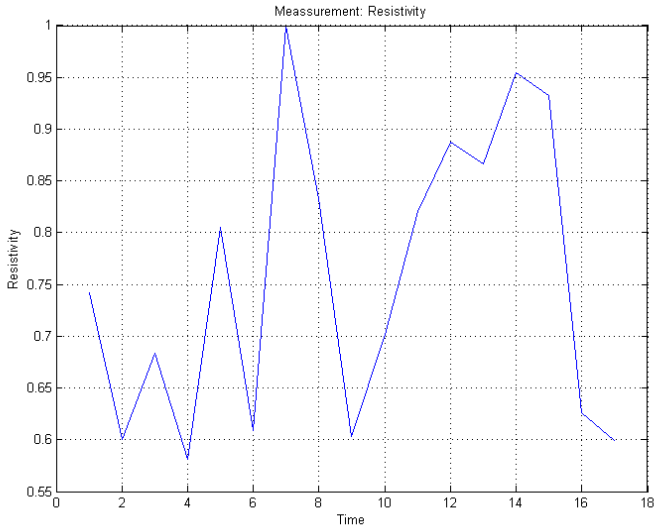

Figure 1.2: Resisitiviy measurements of the finished product from a typical Elkem calcining furnace for a one-week period during 2016. The data is normalized to anonymize it.

The resistivity is obtained by manually choosing the set points for the power and discharge controllers. This can be challenging, and the operator must be careful when changing the inputs. Especially considering the long time constant in the system. It takes a long time from the operator makes a change before the results of the change can be observed. Manual control is also very sensitive to process noise and disturbances. The current manual control of the process leads to inconsistent results as can be seen in Figure 1.2.

It is desirable to find a controller for the resistivity. The resistivity of the finished ECA should be inside of a given range. This range depends on the product to be made from the ECA. It is thought that using a model-based approach will be a good way of finding such a controller.

A controller on the resistivity will hopefully lead to more consistent resistivity results. This means that more of the ECA will be in the desired range. Such a controller will also eliminate most of the human errors the operators might introduce. The controller may help reduce the power consumption as well, which will be a positive contribution both economically and environmentally.

1.6 Challenges

The main challenge in achieving efficient control lies in finding a satisfactory model. The process is complex, and finding a good model is not trivial.

There are a lot of challenges when modelling a process like this. The process is fairly slow, with a dominant time constant of more than 12 hours. In addition to this, no two furnaces will be exactly alike, and the different furnaces might have vastly different be-

haviours. Initially the controller will be developed with a specific furnace in mind. Some changes to the controller might have to be done for each different furnace.

One of the biggest challenges, are the lack of measurements. There are no continuous temperature measurements in the center of the furnace. This means that there is currently no way to actually validate the temperature distribution inside the furnace. Elkem has made some measurements, but the data are sparse, and can not be entirely trusted. They will, however, provide an indication of whether the model is in the right neighbourhood.

The resistivity of the calcinate (i.e., the product) is measured manually twice a day. This means that there are few measurements, and it might be hard to see the dynamics of the system. Excluding the resistivity, the measurements that are of interest are the operation resistance, the interelectrode current, and the secondary voltage. These are provided with a sampling frequency of an hour, which seems to be sufficiently fast when considering the dominant time constant of more than 12 hours.

While resistivity is a material property, and is not dependent on the size or the shape of the an object, the operation resistance is the electrical resistance in the furnace. This will be dependent on the geometry of the furnace. The relationship between the resistivity and the operation resistance is further described in section 4.4 and section 4.5.

There are no measurements on the furnace in-feed. The in-feed is determined by the discharge rate, such that the furnace at all times is filled with material.

Coating on the furnace walls might lead to uneven mass flow down through the furnace (Elkem Carbon, 2017). This can make the current flow asymmetrical, which in turn might result in large variation in product quality. It might also lead to unpredictable phenomena and behaviour that can be hard to model.

Another great challenge is differences in the raw material. Variations in lump size, moisture and volatile contents may have great impact on the process. The fraction of naturally occurring graphite, and the number of cross-links are of great importance as well. The importance of the cross-links are discussed in more detail in Section 2.1.3.

Figure 1.3 shows that the resistivity-temperature curves are vastly different for different raw materials, both in slope and value. This illustrates the effect the differences in the anthracite may have on the process.

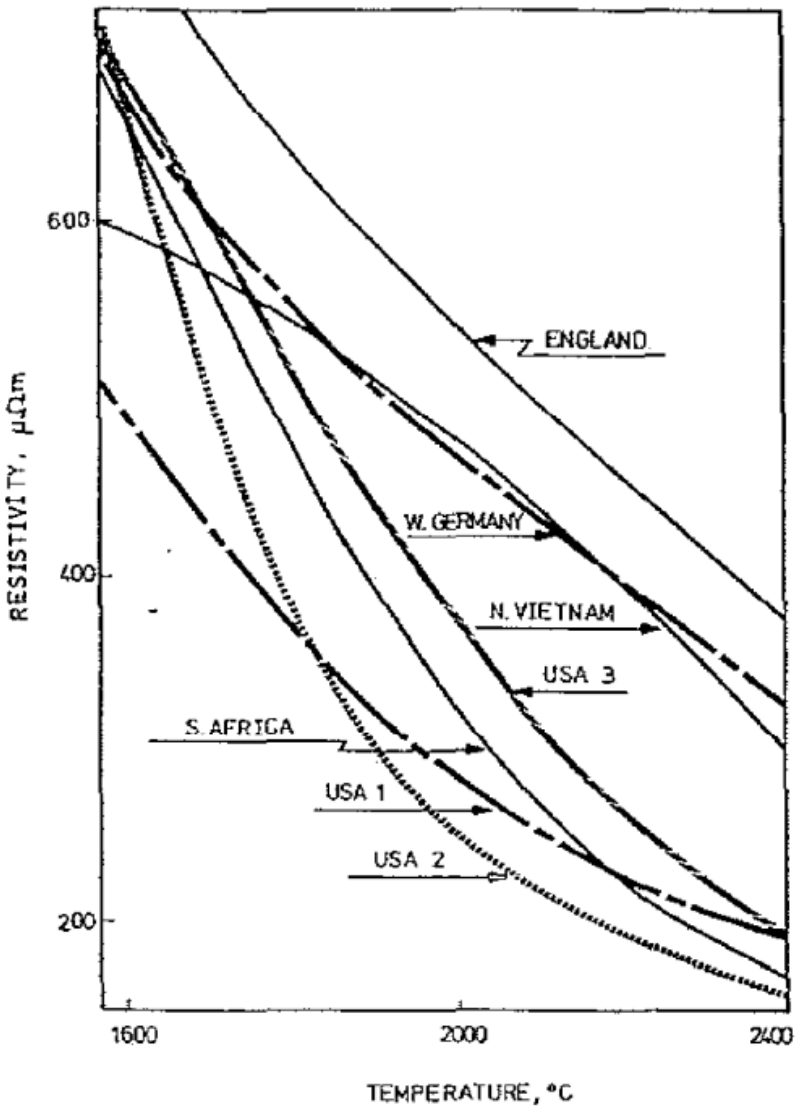

Figure 1.3: Resistivity-temperature plot for anthracite with different origins. From Elkem Carbon (2017).

Chapter 2

Basic Theory

In this chapter an introduction to the basic theory used in this work is given. This theory includes carbon structure and properties, general mass and energy balances, heat transfer, and model predictive control. The sections about mass and energy balances, and heat transfer was also used in Wilson (2016).

This will only be a brief introduction to each of these topics, and will not give a complete understanding. For more information, see the literature cited. There are also a lot more literature on each subject that is not cited.

2.1 Carbon structure and properties

Solid carbons can be categorized into two groups, graphitic carbons and non-graphitic carbons (Gundersen, 1998). Both these are made up of carbon atoms in two dimensional hexagonal networks. The principal difference is that non-graphitic carbon doesn't have any crystallographic order in the third direction, while graphitic carbon does (Edwards et al., 2013).

The non-graphitic carbon is in turn divided into two categories: graphitizable carbons, called soft carbons, and non-graphitizable carbons, called hard carbons (Gundersen, 1998).

2.1.1 Graphite and graphitization

Graphite is made up of layers of the two dimensional hexagonal carbon networks mentioned above. These layers are held together by weak van der Waals forces and are shifted in relation to each other, as illustrated in Figure 2.1. This is known as an ABAB-sequence. At room temperature the unit cell dimension is $a = 2.456$ Å within the layers. The spacing between layers is $d = \frac{c}{2} = 3.354$ Å, where c is the the unit cell height.

Graphitization is the process of turning non-graphitic carbon into graphite by heat treatment, see Figure 2.2. Soft carbons can be fully graphitized by heat treatment alone. Hard carbons can only be fully graphitized during treatment at both high temperature and pressure (Gundersen, 1998).

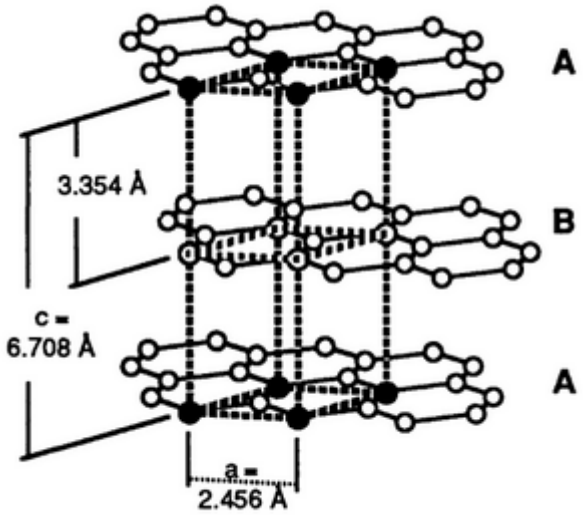

Figure 2.1: Hexagonal unit cell of graphite. From Edwards et al. (2013).

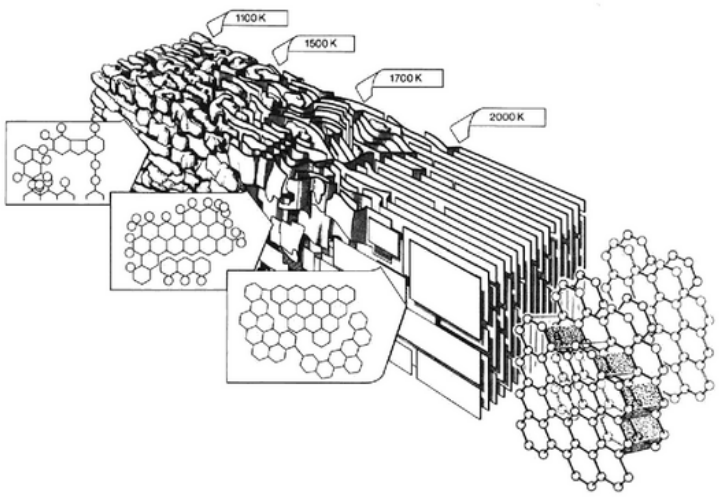

Figure 2.2: Marsh-Griffiths model of graphitization process. From Edwards et al. (2013).

The degree of graphitization (DOG) g is such that $g = 0$ for completely misoriented regions, and $g = 1$ for completely oriented regions. Murty et al. (1969) suggests that the kinetics of the graphitization follows the equation

$$\frac{\mathrm{d}g_0}{\mathrm{d}t} = -n\alpha^{-\frac{1}{n}} g_0^{1+\frac{1}{n}} \tag{2.1}$$

where $g_0 = 1 - g$, n is a constant. α obeys the relation

$$\alpha = \alpha_0 e^{\frac{Q}{RT}} \tag{2.2}$$

where α_0 is a constant, $Q = \frac{E}{n}$ where E is the activation energy, $R = 8.314\ \mathrm{J/(mol\,K)}$ is the gas constant, and T is the temperature. According to Murty et al. (1969) $E = 230 \pm 15\ \mathrm{kcal/mol} = 962.3 \pm 62.8\ \mathrm{kJ/mol}$ for graphitization of coke.

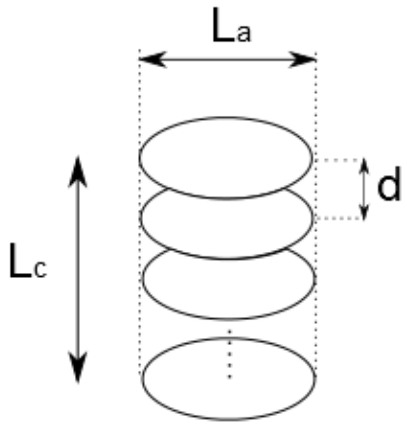

Figure 2.3: A crystallite contains mutually ordered graphite layers. L_a, L_c and d are used to describe the crystallites geometry. Adapted from Gundersen (1998).

2.1.2 Non-Graphitic carbon

The following subsection is based on Gundersen (1998) when not otherwise stated.

A crystallite is a small imperfectly formed crystal. Carbons are made up of microcrystallites that are randomly connected by valence bonds. These crystallites are similar to graphite. They contain layer planes stacked on top of each other held together by van der Waals froces. The parameters usually used for describing the crystallite dimension is

- d_{002} - Interlayer spacing
- L_a - Stack width

- L_c - Stack height

and are illustrated in 2.3. Average values for these parameters can be found by X-ray diffraction, which is described in Warren (1941).

Soft carbons consists of crystallites that are nearly parallel, with weak crosslinks between layer planes. This gives a carbon with an anisotropic structure. In hard carbons there are a strong network of crosslinks between randomly oriented crystallites. Hard carbons have an isotropic structure. The difference between the two structures are illustrated in Figure 2.4. L_c increases with graphitization (Meisingset, 1995), and can be used as a parameter determining DOG.

An assembly of crystallites with more or less the same orientation is called a macrocrystal, see Figure 2.5. The macrocrystal can often be order of magnitudes larger than the crystallites.

2.1.3 Anthracite

Coal is an organic sedimentary rock consisting of carbon, hydrogen, nitrogen, oxygen, sulfur, and traces of other elements (Speight, 2005). Coal rank is a common way of indicating coal structure. Coal rank is in which degree the original plant material has been transformed into carbon, meaning that it is an indication of the carbon content. There are higher oxygen content and some ether linkages in low rank coals compared to medium to high rank coals (Burgess-Clifford et al., 2009). Anthracite is the highest rank of coal. It contains 86-98 wt.% carbon, and the moisture is under 15 wt.% (Bowen and Irwin, 2008; Speight, 2005). The carbon is mostly arranged in large polycyclic aromatic sheets (Burgess-Clifford et al., 2009; Andrésen et al., 2004).

Anthracite is a non-graphitic carbon that behaves like, and have microporosity typical of, hard carbons when thermally treated below 2000 °C (Brandtzæg, 1985). It behaves like soft carbons above 2500 °C (Brandtzæg, 1985; Andrésen et al., 2004). Burgess-Clifford et al. (2009) suggests that there must be two factors present for the anthracite to graphitize:

- The carbon structure must be partially aligned.
- Certain metals must be present as a catalyst.

Further Burgess-Clifford et al. (2009) says that non-graphitic carbon only can be graphitized if the crystallites have cross links that break with sufficient thermal treatment. They also say that the graphitization is much less likely to occur if there are many cross-links between layers, regardless of the catalyst. This implies that some anthracite will be less graphitized than others under the same conditions, just caused by differences in the structure.

There are mainly two different ways of graphitize anthracite yielding two different products, gas calcined anthracite (GCA) and electrically calcined anthracite (ECA). In the GCA process a fuel gas is heated which in turn heats up the anthracite. In the ECA process electric current is passed through the anthracite, warming it by ohmic heating. The temperatures in the GCA process is much lower than those in the ECA process.

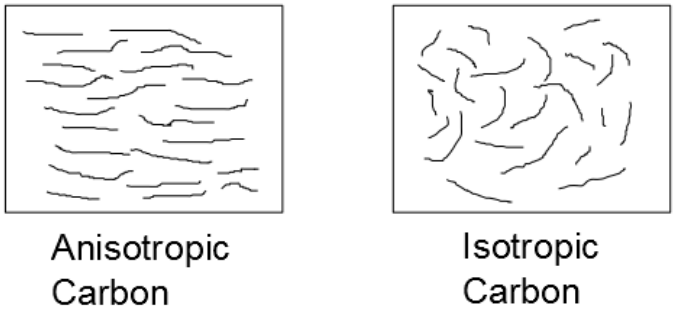

Figure 2.4: Schematic representation of the orientation of the graphitic layers anisotropic and isotropic carbons.

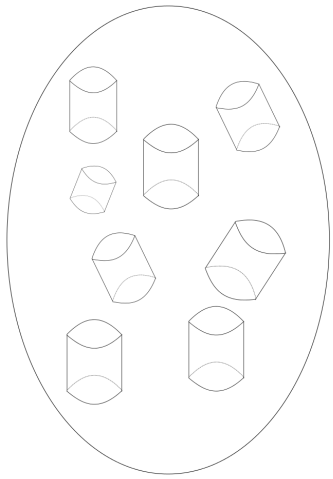

Figure 2.5: Schematic representation of a macrocrystal. The small cylinders are crystallites.

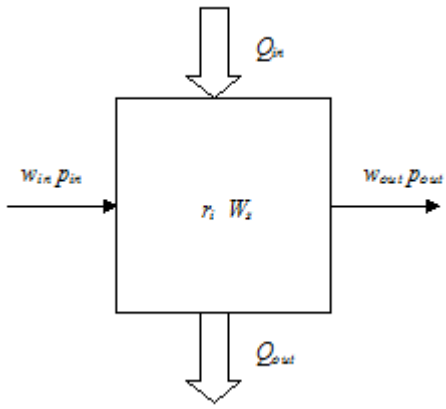

Figure 2.6: General control volume with reactions, mass and energy flows.

2.2 Mass and Energy balance

The general mass balance over a control volume V (see Figure 2.6) is given in Sælid (1984) as

$$\frac{\mathrm{d}}{\mathrm{d}t}\iiint_V \rho_d \, dV = -\iint_A \rho_d \mathbf{v}^{\mathrm{T}} \mathbf{n} \, dA + r \tag{2.3}$$

where ρ_d is the density, $\mathbf{v}$ is the velocity vector of the substance, n is the outwards normal to the surface, dA is an surface element, and r is the reaction rate. For each element i in a control volume, the mass balance can be written as

$$\frac{\mathrm{d}m_i}{\mathrm{d}t} = w_{in,i} - w_{out,i} + \sum_{j=1}^{n_{r,i}} r_{j,i}. \tag{2.4}$$

$w_{in,i}$ and $w_{out,i}$ is the mass flow of substance i in and out of the control volume respectively. $n_{r,i}$ is the number of reactions for substance i.

Sælid (1984) also gives the general energy balance

$$\frac{\mathrm{d}}{\mathrm{d}t}\iiint_V \rho_d e \, dV + \iint_A \rho_d \mathbf{v}^{\mathrm{T}} \mathbf{n} e \, dA = Q - W \tag{2.5}$$

with Q being the net heat transferred into the volume, and W the work done to the surroundings. e is the specific energy given as

$$e = u + \frac{1}{2}v^2 + gz \tag{2.6}$$

where $u = H - \frac{p}{\rho_d}$ is the specific internal energy, p is the pressure, H is the chemical enthalpy, $v = |\mathbf{v}|$, g is the acceleration of gravity, and z is the vertical coordinate. The work is divided into two components

$$W = W_s + \iint_A \mathbf{v}^{\mathrm{T}} \mathbf{n} p \, dA \tag{2.7}$$

where W_s is all other work that is not pressure work, e.g. friction. This means that the energy balance can be written as

$$\frac{\mathrm{d}}{\mathrm{d}t} \iiint_V \rho_d e \, dV + \iint_A \rho_d \mathbf{v}^{\mathrm{T}} \mathbf{n} (e + \frac{p}{\rho_d}) \, dA = Q - W_s. \tag{2.8}$$

Assuming $e \approx u$ the energy balance over a control volumes becomes

$$\begin{aligned} \frac{\mathrm{d}(um)}{\mathrm{d}t} &= H_{in} w_{in} - H_{out} w_{out} + Q - W_s \\ m\frac{\mathrm{d}u}{\mathrm{d}t} + u\frac{\mathrm{d}m}{\mathrm{d}t} &= H_{in} w_{in} - H_{out} w_{out} + Q - W_s \\ m\frac{\mathrm{d}u}{\mathrm{d}t} &= H_{in} w_{in} - H_{out} w_{out} + Q - W_s - u\frac{\mathrm{d}m}{\mathrm{d}t}. \end{aligned} \tag{2.9}$$

2.3 Heat transfer

All background information presented in this section is found in Bergman et al. (2011, p. 2-10). There are three fundamental types of heat transfer: conduction, convection and radiation.

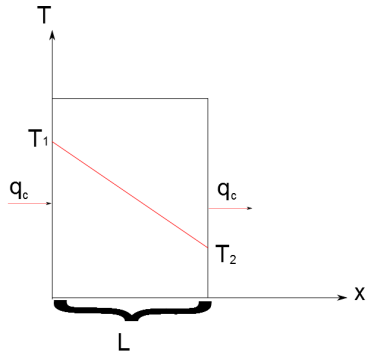

Figure 2.7: Heat transfer by conduction

2.3.1 Conduction

Conduction can be said to be heat transfer that occur across a medium. Inside a solid material, conduction will be the only type of heat transfer. The heat rate by conduction q_c [W] through the medium is

$$q_c = \frac{k}{L} A(T_1 - T_2) \tag{2.10}$$

where k [W/(m K)] is the thermal conductivity, which is a transport property of the material. L [m] is the length through the material, and A [m^2] is the cross section area in the direction of the heat transfer (see Figure 2.7). T_1 [K] and T_2 [K] is the temperatures on the different sides of the medium.

2.3.2 Convection

Convection is used to describe the heat transfer that comes from the movement of a fluid. This is usually classified as either forced convection or free convection. Forced convection is when the fluid flow is caused by a external force, e.g. a pump. Free convection on the other hand is caused by buoyancy forces, that comes from density differences caused by temperature gradients. Both convection and conduction could be methods of heat transfer inside a fluid. The heat rate by convection $q_{c'}$ [W] from the surface to the fluid is

$$q_{c'} = Ah(T_s - T_\infty) \tag{2.11}$$

with A [m^2] being the area between the surface and the fluid, h [W/(m^2 K)] is the convection heat transfer coefficient, T_s [K] is the surface temperature, and T_∞ [K] is the temperature in the fluids outer flow.

2.3.3 Radiation

Emittance of energy through electromagnetic waves is called radiation. All surfaces with temperature above absolute zero radiate. This means that there is a heat transfer between two surfaces with different temperatures, even if there is no intervening medium. The heat rate from one surface to its surroundings q_r [W] is given as

$$q_r = \epsilon A \sigma (T_s^4 - T_{sur}^4). \tag{2.12}$$

Here A [m^2] is the surface's area, $0 \leq \epsilon \leq 1$ is a radiative property of the surface called emissivity, and $\sigma = 5.67 \times 10^{-8}$ [W/(m^2 K^4)] is the Stefan-Boltzmann constant. T_s [K] and T_{sur} [K] is the temperatures of the surface and the surroundings respectively.

2.4 Model predictive control

Model predictive control (MPC) is an advanced control scheme, where the current state of the plant is used as the initial state to solve a finite horizon open loop optimization problem at each sampling instant (Mayne et al., 2000). The optimization problem consists of an cost function to be optimized, subject to relevant constraints. The constraints include a

mathematical model describing the plant behaviour, and may also include operational constraints, e.g. limits on the acceptable ranges of plant variables. Solving the optimization problem gives the optimal input sequence, and the first input in this sequence is applied to the plant.

The great benefit of MPC is that it handles constrains in a really efficient way. It is also easily applied to multiple input, multiple output (MIMO) systems. Foss and Heirung (2013) give a good introduction to MPC.

It is usual to distinguish between linear and nonlinear model predictive control (NMPC). In linear MPC, linear models and constrains are used, and there is a quadratic or linear cost function. In NMPC nonlinear constrains (the model is included in the constraints) are used, and/or there is a non-quadratic cost function (Findeisen et al., 2003). The most common NMPC have a quadratic cost function, and nonlinear constraints. This will be the only instance of NMPC that is considered in this work.

2.4.1 Nonlinear model predictive control

In this work a NMPC formulation using a nonlinear model will be used. The rest of the constrains will be linear, and the cost function quadratic. A mathematical formulation of such a NMPC problem based on Foss and Heirung (2013) is given as

$$\min_{\xi} h(\xi) = \sum_{k=0}^{N-1} \frac{1}{2}\mathbf{z}_{k+1}^{\mathrm{T}}\boldsymbol{Q}_{k+1}\mathbf{z}_{k+1} + \frac{1}{2}\mathbf{u}_k^{\mathrm{T}}\boldsymbol{R}_k\mathbf{u}_k + \frac{1}{2}\boldsymbol{\Delta}\mathbf{u}_k^{\mathrm{T}}\boldsymbol{S}_k\boldsymbol{\Delta}\mathbf{u}_k \tag{2.13a}$$

$$\text{s.t.} \quad \mathbf{x}_{k+1} = f(\mathbf{x}_k, \mathbf{u}_k) \tag{2.13b}$$

$$\mathbf{z}_{min} \leq \mathbf{z}_k \leq \mathbf{z}_{max} \tag{2.13c}$$

$$\mathbf{u}_{min} \leq \mathbf{u}_k \leq \mathbf{u}_{max} \tag{2.13d}$$

$$\boldsymbol{\Delta}\mathbf{u}_{min} \leq \boldsymbol{\Delta}\mathbf{u}_k \leq \boldsymbol{\Delta}\mathbf{u}_{max} \tag{2.13e}$$

$$\mathbf{z}_0 = g(\mathbf{x}_0), \quad \mathbf{x_0} \text{ given} \tag{2.13f}$$

The controlled variable (CV) $\mathbf{z_k} \in \mathbb{R}^{nz}$ at time τ_k, is related to the states $\mathbf{x}_k \in \mathbb{R}^{nx}$ through a measurement function $g : \mathbb{R}^{nx} \to \mathbb{R}^{nz}$ as

$$\mathbf{z}_k = g(\mathbf{x}_k). \tag{2.14}$$

It should be noted that in (2.13), deviation variables are used for z_k. This means that z_k actually refers to the deviation between the variable value and its set point: $z_k - z_{k,ref}$. This is done for convenience in the equations.

The manipulated variable (MV), also called inputs, at time τ_k is denoted $\mathbf{u}_k \in \mathbb{R}^{nu}$. The change in MV is

$$\boldsymbol{\Delta}\mathbf{u}_k = \mathbf{u}_k - \mathbf{u}_{k-1}. \tag{2.15}$$

The nonlinear model is given by (2.13b), where $f : \mathbb{R}^{nx} \times \mathbb{R}^{nu} \to \mathbb{R}^{nx}$ is a nonlinear function.

The matrices $\boldsymbol{Q}_k \in \mathbb{R}^{nz \times nz}$, $\boldsymbol{R}_k \in \mathbb{R}^{nu \times nu}$ and $\boldsymbol{S}_k \in \mathbb{R}^{nu \times nu}$ are penalty matrices whose purpose is to weight certain element in the objective function relative to others at

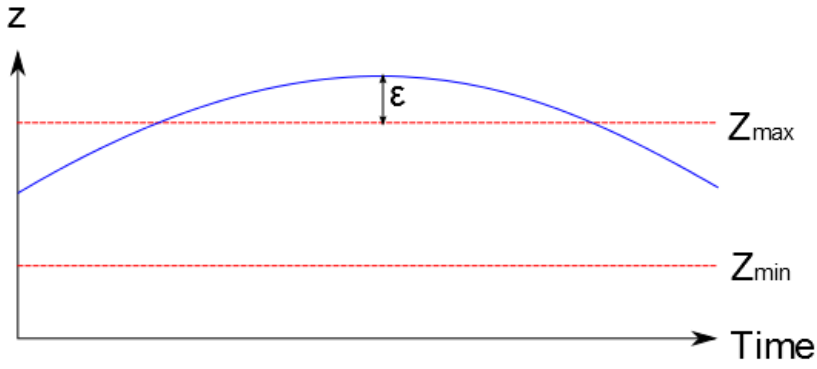

Figure 2.8: Slack variable used in soft constraints. ε is the slack variable, and z the output.

time τ_k. They penalize the deviation from the set points, the inputs and the change in inputs respectively. N is the prediction horizon which is optimized over.

2.4.2 Soft constraints

A big problem for the NMPC controller formulated in (2.13), is that the optimization problem might be infeasible (Maciejowski, 2002). This means that the problem is not able to satisfy all the constraints at the same time. If the problem is feasible the opposite is true: all the constraints are kept.

To illustrate, a big disturbance might take the plant away from the feasible region, and constraints on the inputs prevents the controller to bring the plant back to a feasible region in one iteration. One way of prevent such an infeasibility is to introduce soft constraints.

Soft constraints means that instead of the constraints being strict boundaries that never can be crossed (hard constrains), they can be crossed, but only if it is really necessary. Input constraints often reflect physical properties of the actuators and are seldom possible to soften (Hovd and Stoican, 2014). E.g. a valve can never be opened more than 100 %. It is more usual to soften output constraints.

An easy way of softening constraints is to introduce a slack variable $\boldsymbol{\varepsilon} \in \mathbb{R}^{nz}$, see Figure 2.8. This slack variable should be non-zero only when the constraints are violated, and be heavily penalized in the cost function, so the optimizer keeps them zero if possible.

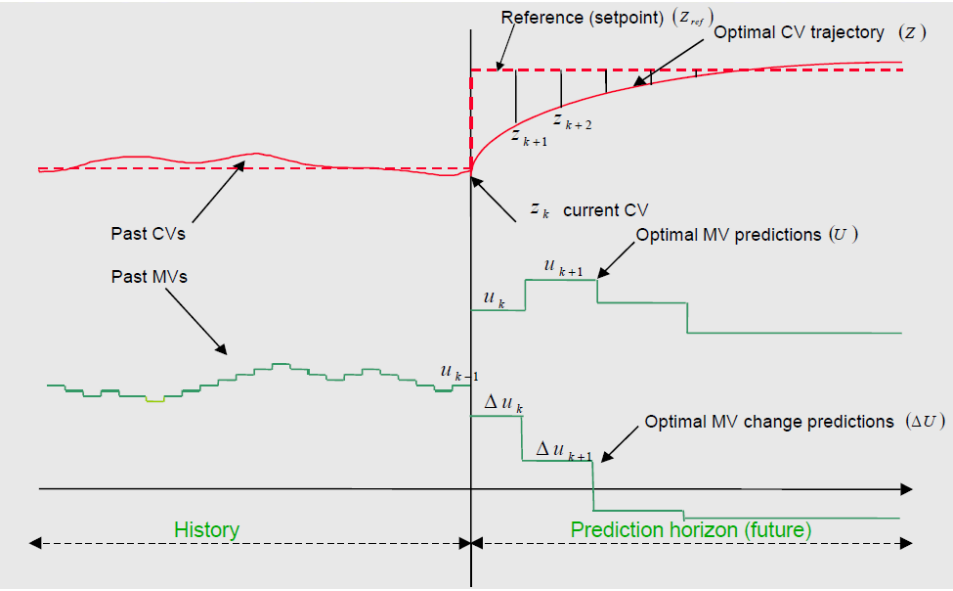

Figure 2.9: MPC trajectory with input blocking. From Dyrset and Hauger (2015).

The new NMPC problem with soft constraints can be formulated as

$$\min_{\xi} h(\xi) = \sum_{k=0}^{N-1} \frac{1}{2}\mathbf{z}_{k+1}^{\mathrm{T}}\boldsymbol{Q}_{k+1}\mathbf{z}_{k+1} + \frac{1}{2}\mathbf{u}_k^{\mathrm{T}}\boldsymbol{R}_k\mathbf{u}_k + \frac{1}{2}\boldsymbol{\Delta}\mathbf{u}_k^{\mathrm{T}}\boldsymbol{S}_k\boldsymbol{\Delta}\mathbf{u}_k + \frac{1}{2}\boldsymbol{\varepsilon}_k^{\mathrm{T}}\boldsymbol{P}_k\boldsymbol{\varepsilon}_k + \mathbf{p}_k^{\mathrm{T}}\boldsymbol{\varepsilon}_k \tag{2.16a}$$

$$\text{s.t.} \quad \mathbf{x}_{k+1} = f(\mathbf{x}_k, \mathbf{u}_k) \tag{2.16b}$$

$$\mathbf{z}_{min} - \boldsymbol{\varepsilon}_k \leq \mathbf{z}_k \leq \mathbf{z}_{max} + \boldsymbol{\varepsilon}_k \tag{2.16c}$$

$$0 \leq \boldsymbol{\varepsilon}_k \leq \boldsymbol{\varepsilon}_{max} \tag{2.16d}$$

$$\mathbf{u}_{min} \leq \mathbf{u}_k \leq \mathbf{u}_{max} \tag{2.16e}$$

$$\boldsymbol{\Delta}\mathbf{u}_{min} \leq \boldsymbol{\Delta}\mathbf{u}_k \leq \boldsymbol{\Delta}\mathbf{u}_{max} \tag{2.16f}$$

$$\mathbf{z}_0 = g(\mathbf{x}_0), \quad \text{given} \tag{2.16g}$$

$\boldsymbol{\varepsilon}_{max}$ is often set to "infinity" (a very large number in practice) to ensure feasibility. $\boldsymbol{P}_k \in \mathbb{R}^{nz \times nz}$ is the penalty matrix of the quadratic cost of $\boldsymbol{\epsilon}_k$, while $\mathbf{p}_k \in \mathbb{R}^{nz}$ is the penalty vector of the linear cost of $\boldsymbol{\epsilon}_k$. Choosing the elements in $\mathbf{p}_k$ sufficiently large can make the soft constraints exact, which means that the constraints will not be breached unless there are no other feasible solutions (Hovd and Braatz, 2001).

2.4.3 Input blocking

The following subsection is based on Cagienard et al. (2007).

A challenge for the MPC controller is its large computational complexity. The complexity of the optimization corresponds with the degrees of freedom. The degrees of freedom come from multiplying the numbers of independent variables with the prediction horizon. To lower the degrees freedom, a common solution is to fix the inputs to be constant over a number of time-steps. This method is called input blocking. Input blocking is illustrated in Figure 2.9

As an example consider a system with 3 inputs and a control horizon of 10 samples. This yields a problem with 30 degrees of freedom. If the inputs are blocked into for instance 4 blocks, the problem will be reduced to 12 degrees of freedom. Note that the input blocks don't have to be of the same size. For instance the blocks may be increasing in size, e.g. 1, 2, 3, 4 samples respectively.

Cagienard et al. (2007) suggests other blocking schemes, but input blocking is sufficient for most application, and will be the only one considered in this work.

Chapter 3

Software

This chapter gives a brief overview of the different pieces of software that is used in this work. The model is implemented in the C programming language. Cybernetica's framework for models written in C is used when implementing the model, meaning that the model automatically gets compliant with all Cybernetica's tools. C is a well known programming language, and it will not be described in this work. Many books are written on the subject, e.g. see Ritchie et al. (1988).

All plots are generated in MATLAB. MATLAB is also well known software, and will not be described here. See for example Moore (2014) for more information.

In this chapter the focus will be on Cybernetica's software and tools. The three tools that are relevant for this work is ModelFit, RealSim and CENIT. Further information on the tools can be found in Cybernetica (2017).

3.1 Cybernetica ModelFit

Cybernetica ModelFit is an off-line estimation tool for state and parameter estimation. It is also a process simulator, and is used for model validation.

Off-line parameter estimation is essential to achieve a good match between a developed model, and process data from a real process. ModelFit uses a sum of squares program on the form

$$\min_{\theta} \sum_{k=1}^{ny} (\hat{y}_k - y_k)^2 \tag{3.1}$$

for parameter estimation. Here $\hat{y}_k$ is the model's computed measurement, while y_k is the measurement from the real process; both for sample k. ny is the number of valid measurements, and θ is the subset of parameters that should be estimated. The estimator can also estimate initial states using the same procedure.

ModelFit is a process simulator as well as an estimation tool. This is useful because the model can be simulated immediately after finding new parameters, making ModelFit well-

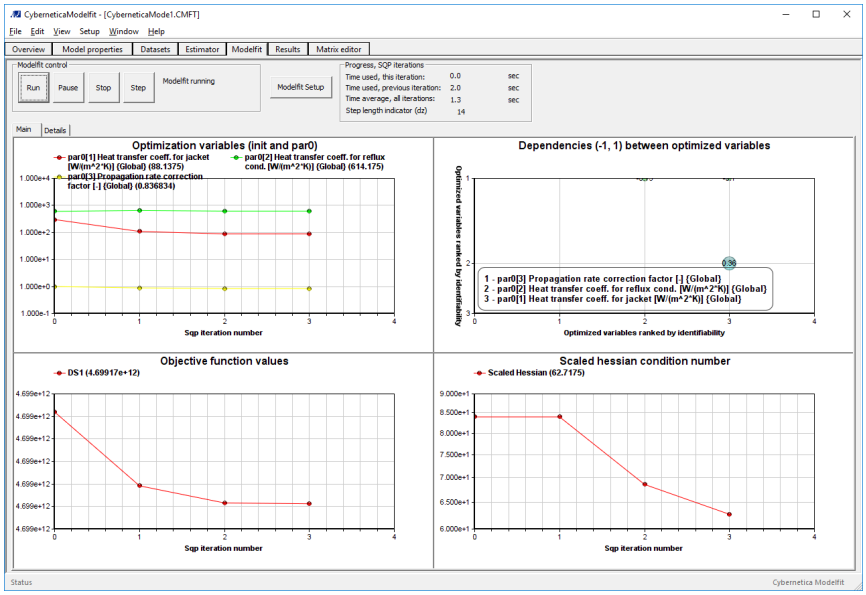

Figure 3.1: Cybernetica ModelFit interface. From Cybernetica (2017).

suited for model validation. It has built-in differential-algebraic equation (DAE) solvers. The solvers range from simple numerical Euler integration, to more sophisticated solvers as CVODE, which is described in detail in Hindmarsh and Serban (2004). It is also possible to design custom solvers that can be used with ModelFit.

3.2 Cybernetica RealSim

Cybernetica RealSim is a process simulator. It is used as a plant replacement when testing CENIT and other control applications. It communicates over the Open Platform Communication (OPC) protocol, which is widely used in the process industry. This to replicate the plant's distributed control system (DCS) as closely as possible.

RealSim is often used during development and for factory acceptance tests (FAT). In a factory implementation RealSim logs the the plant's behavior.

3.3 Cybernetica CENIT

As mentioned in Section 1.2.1 Cybernetica CENIT is Cybernetica's main product. It is powerful and versatile software for NMPC. It consist of two parts: the CENIT Kernel and the CENIT MMI (man-machine interface).

The CENIT Kernel is the part that calculates the controller inputs. It also contains an estimator. It uses OPC to communicate with the plant's control system. As an optional feature, it can communicate with a database to store operational data. This is very useful

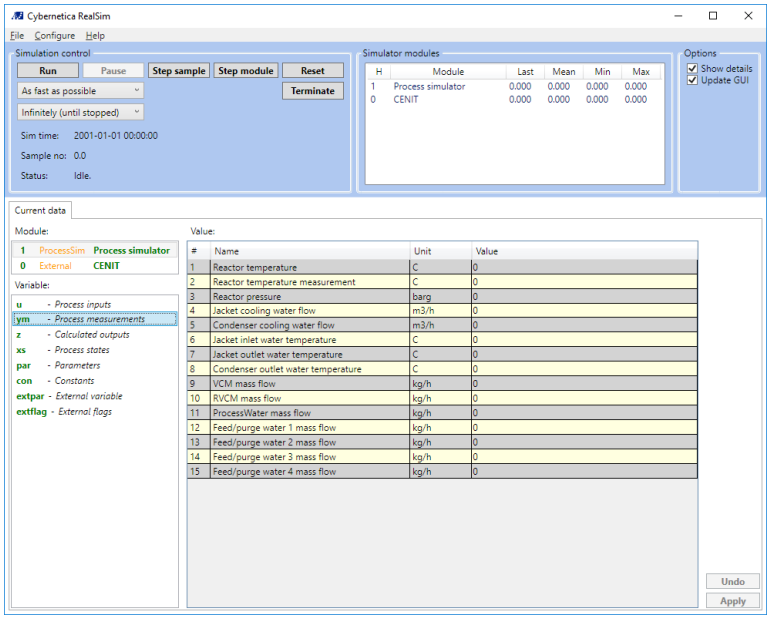

Figure 3.2: Cybernetica RealSim interface. From Cybernetica (2017).

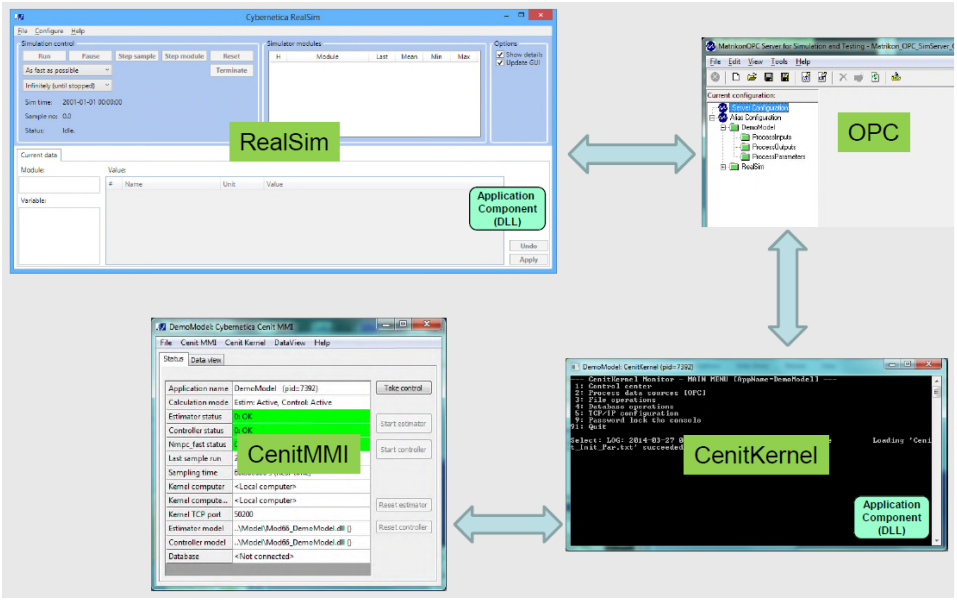

Figure 3.3: Interconnection between Cyberenetica's software. From Dyrset and Hauger (2015).

for off-line analysis of the controller.

The CENIT MMI is a graphical user interface (GUI) used to manage the Kernel. It communicates with the CENIT Kernel through TCP/IP.

The reason why CENIT is divided in this way, is that the CENIT Kernel has to be run on a computer at the plant, while it is very useful to be able to use the CENIT MMI from somewhere else. In this way the control engineer is not dependent on being at the plant.

Figure 3.3 show the interconnection between RealSim and CENIT. In a factory implementation RealSim is replaced with the plant.

Chapter 4

Model

In Box (1979) it is claimed that all models are wrong, but some are useful nevertheless. It is the model builders purpose to make a useful model that is at the same time as simple as possible. Because all models are wrong, it is important to focus on the things that can cause significant errors (Box, 1976), many assumptions can be made without compromising the usefulness of the model.

In the specific case of developing a model of Elkem's electric calciner the most important thing is that it is valid in the range of normal operation. It is unimportant how good the model is in a range where the furnace will not operate.

Most of the development of the model is done in Wilson (2016). For convenience the development and the model will be shown in this chapter. The changes done to the model will be stated. Some details from specialization project will be left out, these can be found in Wilson (2016).

In the furnace to be modelled there are large temperature gradients in the furnace, both in vertical and horizontal direction. The resistivity will change when the anthracite goes down through the furnace. There will also be big differences in the resistivity of the anthracite in the center of the furnace and the anthracite on the sides. To capture this in the model, the furnace is divided into 12 control volumes as shown in Figure 4.1. From above the furnace look like Figure 4.2. A_{inner}, A_{middle} and A_{outer} are the horizontal cross section area of the inner, middle and outer control volumes respectively.

4.1 Mass balance

The mass balance over a control volume without reactions are trivially found as

$$\frac{\mathrm{d}m_i}{\mathrm{d}t} = w_{in,i} - w_{out,i} \tag{4.1}$$

with m_i [kg] being the mass of control volume $i \in \{1, 2, ..., 12\}$ and $w_{in,i}$ [kg/s] and $w_{out,i}$ [kg/s] being the mass flow in to and out of control volume i respectively. It is assumed that the flow from control volume 6 gets distributed into volume 7 and 11 based

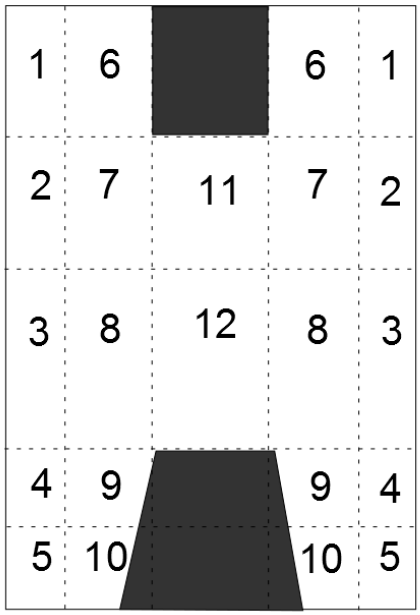

Figure 4.1: Cross section of the furnace seen from the side with control volumes. The black areas are electrodes.

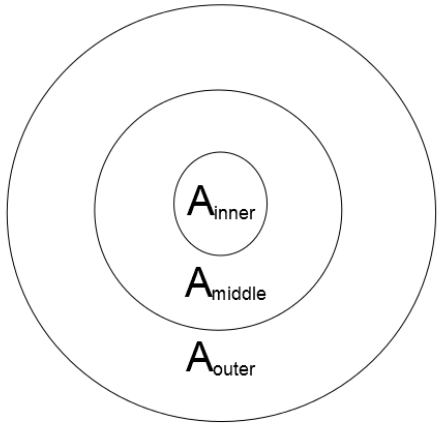

Figure 4.2: Cross section of the furnace seen from above.

on the percentage of the horizontal cross section areas. It is also assumed that all of the mass from control volume 8 and 12 flows into volume 9. For the rest of the control volumes plug flow is assumed. The mass flow is shown in Figure 4.3.

Keeping this in mind and writing (4.1) for each control volume gives the equations

$$\frac{\mathrm{d}m_1}{\mathrm{d}t} = w_{in,1} - w_{out,1} \tag{4.2a}$$
$$\frac{\mathrm{d}m_2}{\mathrm{d}t} = w_{out,1} - w_{out,2} \tag{4.2b}$$
$$\frac{\mathrm{d}m_3}{\mathrm{d}t} = w_{out,2} - w_{out,3} \tag{4.2c}$$
$$\frac{\mathrm{d}m_4}{\mathrm{d}t} = w_{out,3} - w_{out,4} \tag{4.2d}$$
$$\frac{\mathrm{d}m_5}{\mathrm{d}t} = w_{out,4} - w_{out,5} \tag{4.2e}$$
$$\frac{\mathrm{d}m_6}{\mathrm{d}t} = w_{in,6} - w_{out,7} \tag{4.2f}$$
$$\frac{\mathrm{d}m_7}{\mathrm{d}t} = \frac{A_{middle}}{A_{middle} + A_{inner}} w_{out,6} - w_{out,7} \tag{4.2g}$$
$$\frac{\mathrm{d}m_8}{\mathrm{d}t} = w_{out,7} - w_{out,8} \tag{4.2h}$$
$$\frac{\mathrm{d}m_9}{\mathrm{d}t} = w_{out,8} + w_{out,12} - w_{out,9} \tag{4.2i}$$
$$\frac{\mathrm{d}m_{10}}{\mathrm{d}t} = w_{out,9} - w_{out,10} \tag{4.2j}$$
$$\frac{\mathrm{d}m_{11}}{\mathrm{d}t} = \frac{A_{inner}}{A_{middle} + A_{inner}} w_{out,6} - w_{out,11} \tag{4.2k}$$
$$\frac{\mathrm{d}m_{12}}{\mathrm{d}t} = w_{out,11} - w_{out,12} \tag{4.2l}$$

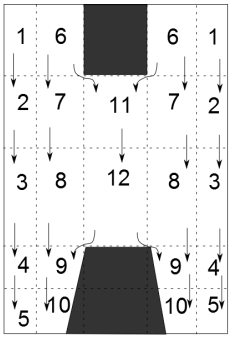

Figure 4.3: Mass flow between control volumes inside the furnace.

4.2 Resistivity

The quality of the calcination can be described by three different parameters:

- DOG, g
- Average crystallite height, L_c
- Electrical resistivity, ρ

The resistivity is measured directly in the process. It is therefore naturally to use this as the calcination parameter. Using the resistivity will also result in the model being more macro property focused. In this work it is desired to look at the macro properties rather than the micro properties when possible.

Brandtzæg et al. (2016) gives a time dependent equation for the electrical conductivity κ as

$$\kappa = b\tau^n e^{\frac{-Q}{RT}} \tag{4.3}$$

where b is a constant, τ is the time, R is the gas constant, and T is the temperature. $Q = nE$, where E is the activation energy and n is a constant. The term effective activation energy will be used for Q. Note that the same constant n is used both in τ^n and in Q.

Inspired by this and (2.1) the change in resistivity is proposed as a temperature dependent reaction

$$s_i = (\rho_i - \rho_s(T, \text{type}))k_\rho e^{\frac{-nE}{RT}} \tag{4.4}$$

where s_i $[\Omega\,\mathrm{m/s}]$ is the reaction rate of control volume i, k_ρ $[1/\mathrm{s}]$ is a reaction rate constant. ρ_i $[\Omega\,\mathrm{m}]$ is the resistivity in control volume i, and $\rho_s(T, \text{type})$ $[\Omega\,\mathrm{m}]$ is a steady state resistivity dependent on the temperature and the raw material; the resistivity is highly dependent on the properties of the raw material that are fed into the furnace as discussed in section 1.6. This reaction is not reversible, meaning that if $s_i < 0$, s_i is set to zero.

The mass will propagate down through the furnace. The resistivity is a material property and will follow the mass. Using a mass balance gives

$$\frac{\mathrm{d}(\rho_i m_i)}{\mathrm{d}t} = w_{in,i}\rho_{in,i} - w_{out,i}\rho_i - m_i s_i \tag{4.5}$$

which solved for $\dfrac{\mathrm{d}\rho_i}{\mathrm{d}t}$ becomes

$$\begin{aligned} m_i\frac{\mathrm{d}\rho_i}{\mathrm{d}t} + \rho_i\frac{\mathrm{d}m_i}{\mathrm{d}t} &= w_{in,i}\rho_{in,i} - w_{out,i}\rho_i - m_i s_i \\ m_i\frac{\mathrm{d}\rho_i}{\mathrm{d}t} &= w_{in,i}\rho_{in,i} - w_{out,i}\rho_i - (w_{in,i} - w_{out,i})\rho_i - m_i s_i \\ \frac{\mathrm{d}\rho_i}{\mathrm{d}t} &= \frac{w_{in,i}}{m_i}(\rho_{in,i} - \rho_i) - s_i \end{aligned} \tag{4.6}$$

Which when written out for each control volume gives the equations

$$\frac{\mathrm{d}\rho_1}{\mathrm{d}t} = \frac{w_{in,1}}{m_1}(\rho_{in} - \rho_1) - s_1 \tag{4.7a}$$
$$\frac{\mathrm{d}\rho_2}{\mathrm{d}t} = \frac{w_{out,1}}{m_2}(\rho_1 - \rho_2) - s_2 \tag{4.7b}$$
$$\frac{\mathrm{d}\rho_3}{\mathrm{d}t} = \frac{w_{out,2}}{m_3}(\rho_2 - \rho_3) - s_3 \tag{4.7c}$$
$$\frac{\mathrm{d}\rho_4}{\mathrm{d}t} = \frac{w_{out,3}}{m_4}(\rho_3 - \rho_4) - s_4 \tag{4.7d}$$
$$\frac{\mathrm{d}\rho_5}{\mathrm{d}t} = \frac{w_{out,4}}{m_5}(\rho_4 - \rho_5) - s_5 \tag{4.7e}$$
$$\frac{\mathrm{d}\rho_6}{\mathrm{d}t} = \frac{w_{in,6}}{m_6}(\rho_{in} - \rho_6) - s_6 \tag{4.7f}$$
$$\frac{\mathrm{d}\rho_7}{\mathrm{d}t} = \frac{A_{middle}}{A_{middle} + A_{inner}} \frac{w_{out,6}}{m_7}(\rho_6 - \rho_7) - s_7 \tag{4.7g}$$
$$\frac{\mathrm{d}\rho_8}{\mathrm{d}t} = \frac{w_{out,7}}{m_8}(\rho_7 - \rho_8) - s_8 \tag{4.7h}$$
$$\frac{\mathrm{d}\rho_9}{\mathrm{d}t} = \frac{w_{out,8}}{m_9}(\rho_8 - \rho_9) + \frac{w_{out,12}}{m_9}(\rho_{12} - \rho_9) - s_9 \tag{4.7i}$$
$$\frac{\mathrm{d}\rho_{10}}{\mathrm{d}t} = \frac{w_{out,9}}{m_{10}}(\rho_9 - \rho_{10}) - s_{10} \tag{4.7j}$$
$$\frac{\mathrm{d}\rho_{11}}{\mathrm{d}t} = \frac{A_{inner}}{A_{middle} + A_{inner}} \frac{w_{out,6}}{m_{11}}(\rho_6 - \rho_{11}) - s_{11} \tag{4.7k}$$
$$\frac{\mathrm{d}\rho_{12}}{\mathrm{d}t} = \frac{w_{out,11}}{m_{12}}(\rho_{11} - \rho_{12}) - s_{12}. \tag{4.7l}$$

The output of the system is the finished product's resistivity ρ_{out}. This is found by taking the weighted average of the resistivity in control volume 5 and 10:

$$\rho_{\text{out}} = \frac{w_{out,5}\rho_5 + w_{out,10}\rho_{10}}{w_{out,5} + w_{out,10}} \tag{4.8}$$

A key difference compared to Wilson (2016) is that now the term $e^{\frac{-nE}{RT}}$ in s_i, where the term $e^{\frac{-E}{RT}}$ was used before. $E = 960\ \mathrm{kJ/mol}$ from Murty et al. (1969) where used. Now $E = 340\ \mathrm{kJ/mol}$ and $n = 0.087$ from Brandtzæg et al. (2016) is used as a starting point for parameter estimation. Since Murty et al. (1969) concerns graphtization of coke, while Brandtzæg et al. (2016) concerns calcination of anthracite it seems reasonable to emphasize the latter. Murty et al. (1969) also does not give any numerical value for n, so the effect might be the same by using $E = 960\ \mathrm{kJ/mol}$ and another value for n.

In the discussion section in Wilson (2016) report it is speculated that the high activation energy used, leads the graphitization reaction to be very temperature sensitive. This in turn leads to very little graphitization in the cold outer and middle control volumes. Now that

the effective activation energy is much lower, this should mean that there is more resistiviy dynamics in all the control volumes, and in the finished product's resistiviy as well.

4.3 Energy balance

Using a general energy balance for each of the control volumes gives the equations

$$\begin{aligned}\frac{\mathrm{d}T_1}{\mathrm{d}t} &= \frac{w_{in,1}(C_{p,in}T_{in} - C_{p,1}T_1) - Q_{1,0} - Q_{1,top} + Q_{2,1} + Q_{6,1}}{c_{p,1}m_1} \\ &+ \frac{-\Delta H_R f_1 s_1 - \Delta H_{R_\gamma} X_{\gamma,1} w_{in,1} - \Delta H_{R_{\mathrm{H_2O}}} X_{\mathrm{H_2O},1} w_{in,1} + P_{c,1}}{c_{p,1}m_1}\end{aligned} \tag{4.9a}$$

$$\frac{\mathrm{d}T_2}{\mathrm{d}t} = \frac{w_{out,1}(C_{p,1}T_1 - C_{p,2}T_2) - Q_{2,3} - Q_{2,1} - Q_{2,0} + Q_{7,2} - \Delta H_R f_2 s_2}{c_{p,2}m_2} \tag{4.9b}$$

$$\frac{\mathrm{d}T_3}{\mathrm{d}t} = \frac{w_{out,2}(C_{p,2}T_2 - C_{p,3}T_3) - Q_{3,4} - Q_{3,0} + Q_{2,3} + Q_{8,3} - \Delta H_R f_3 s_3}{c_{p,3}m_3} \tag{4.9c}$$

$$\frac{\mathrm{d}T_4}{\mathrm{d}t} = \frac{w_{out,3}(C_{p,3}T_3 - C_{p,4}T_4) - Q_{4,5} - Q_{4,0} + Q_{3,4} + Q_{9,4} - \Delta H_R f_4 s_4}{c_{p,4}m_4} \tag{4.9d}$$

$$\begin{aligned}\frac{\mathrm{d}T_5}{\mathrm{d}t} &= \frac{w_{out,4}(C_{p,4}T_4 - C_{p,5}T_5) - Q_{5,bot}}{c_{p,5}m_5} \\ &+ \frac{-Q_{5,0} + Q_{4,5} + Q_{10,5} - \Delta H_R f_5 s_5}{c_{p,5}m_5}\end{aligned} \tag{4.9e}$$

$$\begin{aligned}\frac{\mathrm{d}T_6}{\mathrm{d}t} &= \frac{w_{in,6}(C_{p,in}T_{in} - C_{p,6}T_6) - Q_{6,top} - Q_{6,el} - Q_{6,1} + Q_{7,6}}{c_{p,6}m_6} \\ &+ \frac{-\Delta H_R f_6 s_6 - \Delta H_{R_\gamma} X_{\gamma,6} w_{in,6} - \Delta H_{R_{\mathrm{H_2O}}} X_{\mathrm{H_2O},6} w_{in,6} + P_{c,6}}{c_{p,6}m_6}\end{aligned} \tag{4.9f}$$

$$\begin{aligned}\frac{\mathrm{d}T_7}{\mathrm{d}t} &= \frac{\frac{A_{middle}}{A_{middle}+A_{inner}} w_{out,6}(C_{p,6}T_6 - C_{p,7}T_7) - Q_{7,8}}{c_{p,7}m_7} \\ &+ \frac{-Q_{7,6} - Q_{7,2} + Q_{11,7}P_{el,7} - \Delta H_R f_7 s_7}{c_{p,7}m_7}\end{aligned} \tag{4.9g}$$

$$\begin{aligned}\frac{\mathrm{d}T_8}{\mathrm{d}t} &= \frac{w_{out,7}(C_{p,7}T_7 - C_{p,8}T_8) - Q_{8,9} - Q_{8,3}}{c_{p,8}m_8} \\ &+ \frac{Q_{7,8} + Q_{12,8} + P_{el,8} - \Delta H_R f_8 s_8}{c_{p,8}m_8}\end{aligned} \tag{4.9h}$$

$$\begin{aligned}\frac{\mathrm{d}T_9}{\mathrm{d}t} &= \frac{w_{out,8}(C_{p,8}T_8 - C_{p,9}T_9) + w_{out,12}(C_{p,12}T_{12} - C_{p,9}T_9)}{c_{p,9}m_9} \\ &+ \frac{-Q_{9,10} - Q_{9,4} - Q_{9,el} + Q_{8,9} - \Delta H_R f_9 s_9}{c_{p,9}m_9}\end{aligned} \tag{4.9i}$$

$$\frac{\mathrm{d}T_{10}}{\mathrm{d}t} = \frac{w_{out,9}(C_{p,9}T_9 - C_{p,10}T_{10}) - Q_{10,bot}}{c_{p,10}m_{10}} + \frac{-Q_{10,5} + Q_{10,el} + Q_{9,10} - \Delta H_R f_{10} s_{10}}{c_{p,10}m_{10}} \tag{4.9j}$$

$$\frac{\mathrm{d}T_{11}}{\mathrm{d}t} = \frac{\frac{A_{inner}}{A_{middle}+A_{inner}} w_{out,6}(C_{p,6}T_6 - C_{p,11}T_{11}) - Q_{11,7}}{c_{p,11}m_{11}} + \frac{-Q_{11,12} - Q_{11,el} + P_{el,11} - \Delta H_R f_{11} s_{11}}{c_{p,11}m_{11}} \tag{4.9k}$$

$$\frac{\mathrm{d}T_{12}}{\mathrm{d}t} = \frac{w_{out,11}(C_{p,11}T_{11} - C_{p,12}T_{12}) - Q_{12,8}}{c_{p,12}m_{12}} + \frac{-Q_{12,el} + Q_{11,12} + P_{el,12} - \Delta H_R f_{12} s_{12}}{c_{p,12}m_{12}} \tag{4.9l}$$

Symbol explanations are given in Table 4.1. An example of heat flow in a control volume is shown in Figure 4.4.

Table 4.1: Symbol explanation of (4.9).

Symbol	Unit	Explanation
$Q_{i,el}$	W	Heat from control volume i to the electrode
$Q_{i,top}$	W	Heat from control volume i over the top
$Q_{i,j}$	W	Heat from control volume i to control volume j
$Q_{i,0}$	W	Heat from control volume i out through the wall
$P_{c,i}$	W	Heating power from volatile combustion to control volume i
$P_{el,i}$	W	Heating power from ohmic heating to control volume i
f_i	$\mathrm{kg}/(\Omega\,\mathrm{m})$	Factor determining how much mass that get graphitised
ΔH_R	J/kg	Reaction enthalpy from graphitization
ΔH_{R_γ}	J/kg	Enthalpy from driving off the volatiles
$\Delta H_{R_{\mathrm{H_2O}}}$	J/kg	Enthalpy from vaporizing water
$X_{\gamma,i}$	—	Weight fraction of volatiles driven off in control volume i
$X_{\mathrm{H_2O},i}$	—	Weight fraction of water vaporized in control volume i
$C_{p,i}$	J/K	Heat capacity in control volume i

Here it is assumed that all the water and volatiles is driven off in the top control volumes 1 and 6, and that the ohmic heating happens in the middle control volumes 7, 8, 11 and 12. The rest of the control volumes will be heated up though heat transfer from these volumes. In reality there will be a contribution from ohmic heating in all the control volumes. It is assumed that the contribution from heat transfer will be dominating in all other control volumes. An example is included here to justify this assumption.

Through simulation it was found that $P_{el,11} \approx 750$ [kW] and $P_{el,7} \approx 25$ [kW] for a normal case. This shows that the ohmic heating power is decreasing rapidly when moving away from the center of the furnace. On the other hand for the same case $Q_{11,7} \approx 700$ [kW] and $Q_{7,2} \approx 250$ [kW]. This means that the heat transfer is not decreasing with the same rate as the ohmic heat. $P_{el,11}$ is approximately 30 times greater than $P_{el,7}$. The

contribution of the ohmic heating will decrease even more when considering the control volumes further from the center. Therefore the assumption is probably valid.

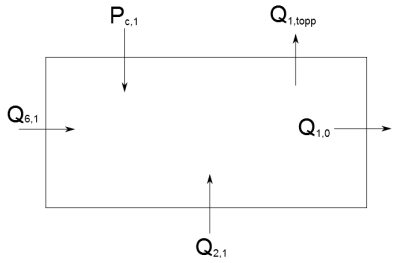

Figure 4.4: Heat flow in control volume 1.

4.4 Electrical model

The furnace's electric circuit consists of a transformer with a primary voltage V_p and a secondary voltage V_s. The secondary circuit consists of the furnace modeled as two resistors $R_{inner} = R_{11} + R_{12}$ and $R_{middle} = R_7 + R_8$ in parallel, and a resistor for the rest of the circuit R_{loss}. This is illustrated in Figure 4.5.

In Wilson (2016) the current is used as input. The ohmic heating for each control volume is then found as

$$P_{el,i} = R_i I_i^2. \tag{4.10}$$

where R_i and I_i is the electrical resistance and current in control volume i respectively. I_i is found through division of current

$$I_7 = I_8 = I_s \frac{R_{11} + R_{12}}{R_7 + R_8 + R_{11} + R_{12}} \tag{4.11a}$$

$$I_{11} = I_{12} = I_s \frac{R_7 + R_8}{R_7 + R_8 + R_{11} + R_{12}}. \tag{4.11b}$$

where I_s is the interelectrode current. It is suggested in Wilson (2016) that maybe the voltage should be used as input instead.

While using voltage as input the ohmic heating in each control volume is found as

$$P_{el,i} = \frac{V_i^2}{R_i}. \tag{4.12}$$

where V_i is the voltage over control volume i. The furnace's equivalent resistance R_{eq} is

$$R_{eq} = \frac{(R_7 + R_8)(R_{11} + R12)}{R_7 + R_8 + R_{11} + R12}. \tag{4.13}$$

The furnace voltage V_{furn} is easily found by division of voltage

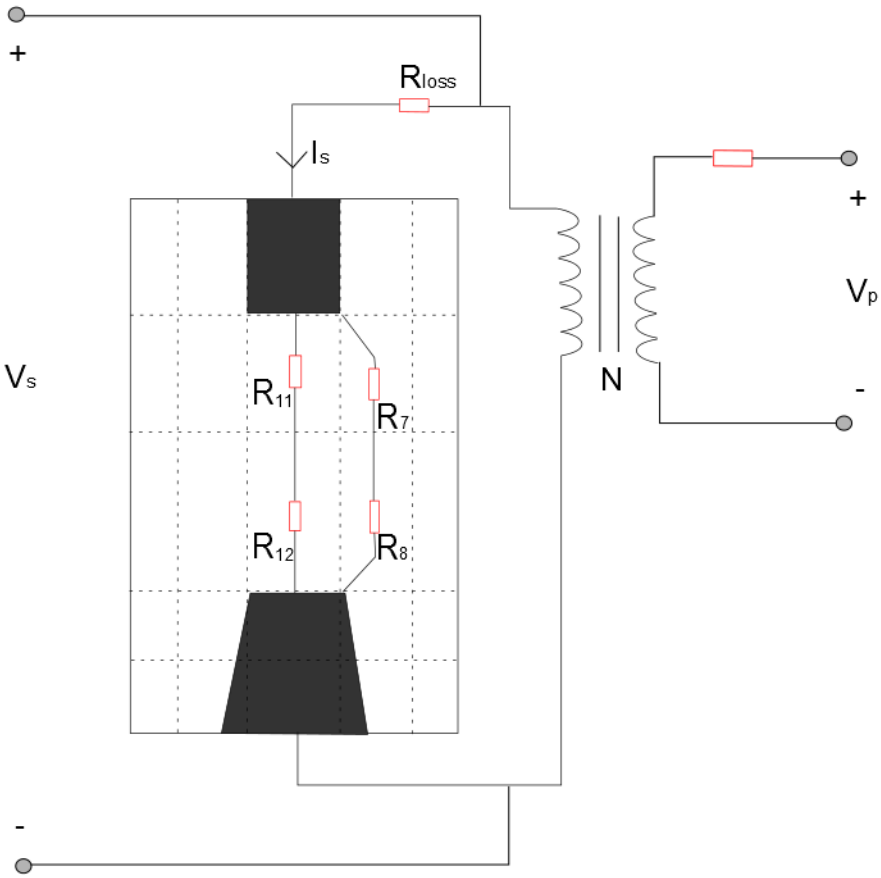

Figure 4.5: Simple schematic of the furnace's electrical system.

$$V_{furn} = V_s \frac{R_{eq}}{R_{eq} + R_{loss}}. \tag{4.14}$$

Further the voltage for each control volume is found by division of voltage

$$V_7 = V_{furn} \frac{R_7}{R_7 + R_8} \tag{4.15a}$$

$$V_8 = V_{furn} \frac{R_8}{R_7 + R_8} \tag{4.15b}$$

$$V_{11} = V_{furn} \frac{R_{11}}{R_{11} + R_{12}} \tag{4.15c}$$

$$V_{12} = V_{furn} \frac{R_{12}}{R_{11} + R_{12}}. \tag{4.15d}$$

Two conflicting phenomenons are introduced to the model depending on which input is used.

When using the current as input the electrical power in the furnaces is found by (4.10). When the resistance decreases, the power decreases, which in turn makes the temperature decrease. Lower temperature leads to less graphitization, which means that the resistivity, and therefore the resistance, increases. When the resistance increases, the power increases, and then the temperature increases. Higher temperature leads to more graphtization and lower resistivity. The whole thing becomes self-stabilizing. There is no indication that this behaviour is present in the furnace. There is however, no direct evidence that this occurs during simulations.

When using the voltage as input the electrical power in the furnace is given by (4.12). Here if the resistance decreases, the power increases. This in turn makes the temperature increase. Higher temperature makes the resistance decrease, which again leads the power to increase. This is an unstable circle. This phenomenon is called thermal runaway. King et al. (1990) examines if thermal runaway is the cause of an observed instability, but concludes that it is unlikely that it is caused by thermal runaway alone. They suggest that the granular flow behavior may have a greater impact.

It is unwanted to introduce nonphysical elements to the model. It is obvious that both of these phenomenons can not represent the physical behaviour. The author has not been able to find any evidence of either of the phenomenons, nor find any litterateur to mention any of the phenomenons with regards to the ECA process, with the exception of King et al. (1990). King et al. (1990) does not state that thermal runaway is present in the process. This suggest that neither of the phenomenons should be introduced in the model.

Thermal runaway was observed in the model as can be seen in Figure 4.7. It was however only possible to observe thermal runaway while using a high effective activation energy. When using more suitable parameters, no thermal runaway could be observed. This means that introducing thermal runaway in the model might not be a problem, even if it is a nonphysical element.

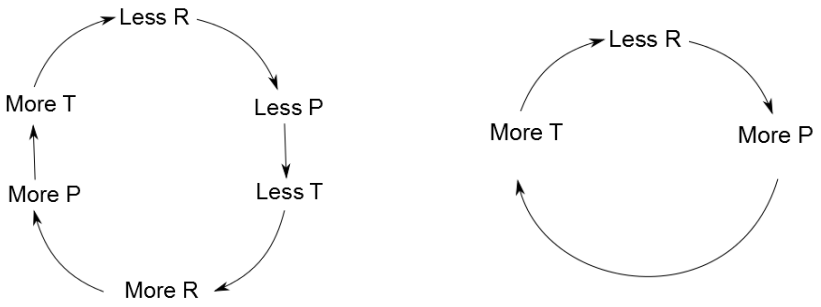

(a) Using current as input: self-stabilization. **(b)** Using voltage as input: thermal runaway.

Figure 4.6: Phenomenons included when choosing different inputs.

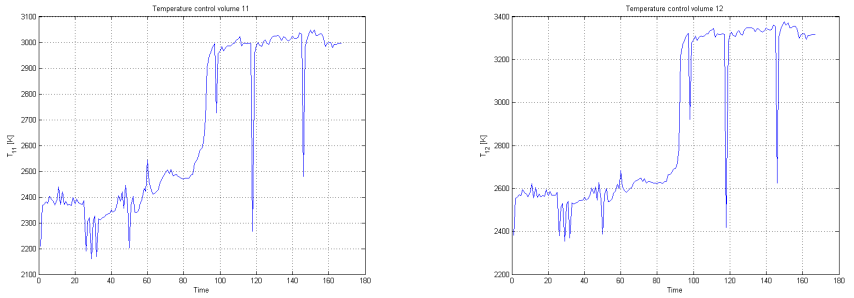

(a) Temperature in control volume 11 during thermal runaway. **(b)** Temperature in control volume 12 during thermal runaway.

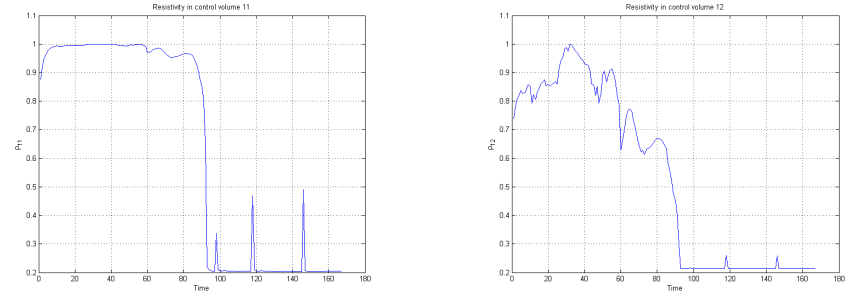

(c) Normalized resistivity in control volume 11 during thermal runaway. **(d)** Normalized resistivity in control volume 12 during thermal runaway.

Figure 4.7: Thermal runaway observed in control volume 11 and 12.

4.5 Bulk resistance

When developing the model in Wilson (2016) the specific resistivity is used when finding the resistance in a control volume. The relationship between resistivity and resistance

$$R = \rho \frac{L}{A}. \tag{4.16}$$

is used directly. In the final report it is suggested to use the bulk resistivity instead to improve the model. The bulk resistivity will depend on the void fraction in the control volume. It is desirable to find the bulk resistance in a control volume as a function of the anthracite's resistivity and the void fraction: $R_{\text{bulk}}(\rho_{\text{A}}, \nu)$. In this section such a bulk resistance is derived.

The resistance of a anthracite particle can trivially be found from (4.16)

$$R_{\text{A}} = \rho_{\text{A}} \frac{h_{\text{p}}}{A_{\text{p}}} \tag{4.17}$$

where h_{p} is the particle height, and A_{p} is the particle's cross section area. Similarly for a void space

$$R_{\nu} = \rho_{\nu} \frac{h_{\nu}}{A_{\nu}} \tag{4.18}$$

where R_{ν} is the void resistance, ρ_{ν} is the void resistivity, h_{ν} is the void height, and A_{ν} is the void cross section area.

The control volume is divided into N_{L} layers where each layer has resistance R_{L}. The total resistance R_{tot} will be all these layers in series

$$R_{\text{tot}} = \sum_{i=1}^{N_{\text{L}}} R_{\text{L}} = N_{\text{L}} R_{\text{L}}. \tag{4.19}$$

The height in the control volume will depend on the stacking of the particles. Including this to the model

$$h_{\text{p}} = \beta r_{\text{p}} \tag{4.20}$$

where r_{p} is the particle radius, and $\sqrt{3} \leq \beta \leq 2$ is a parameter depending on the stacking of the particles. If it is assumed that the particles are perfectly round $\beta = \sqrt{3}$, if it is assumed that the particles are cylinders $\beta = 2$, see Figure 4.9. This in addition to $A_{\text{p}} = A_{\nu} = \pi r_{\text{p}}^2$ gives

$$R_{\text{A}} = \rho_{\text{A}} \frac{\beta \cancel{r_{\text{p}}}}{\pi \cancel{r_{\text{p}}^2}} = \rho_{\text{A}} \frac{\beta}{\pi r_{\text{p}}} \tag{4.21}$$

and

$$R_{\nu} = \rho_{\nu} \frac{h_{\nu}}{\pi r_{\text{p}}^2}. \tag{4.22}$$

Each layer is assumed to be N_{p} particles and voids in parallel as illustrated in Figure 4.8, and the resistance of a layer is computed as

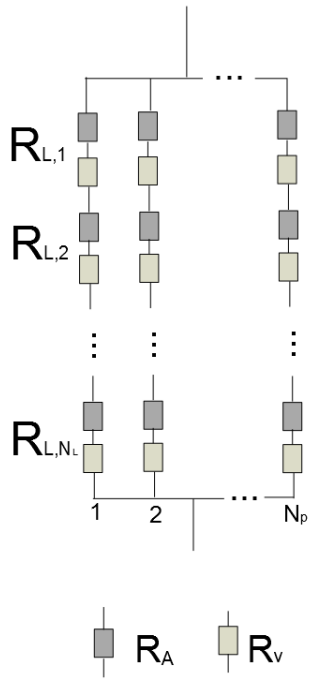

Figure 4.8: Diagram for the equivalent bulk resistance.

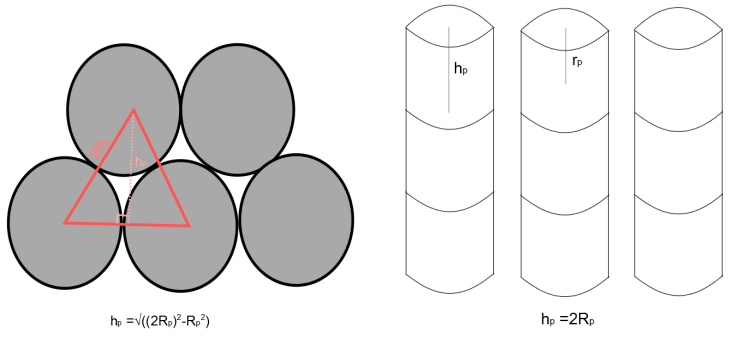

(a) Stacking of circular particles **(b)** Stacking of cylindrical particles

Figure 4.9: Stacking of particles

$$\frac{1}{R_{\mathrm{L}}} = \sum_{i=1}^{N_{\mathrm{p}}} \left(\frac{1}{R_{\mathrm{A}} + R_{\nu}} \right) = \frac{N_{\mathrm{p}}}{(R_{\mathrm{A}} + R_{\nu})}$$

$$\implies R_{\mathrm{L}} = \frac{1}{N_{\mathrm{p}}} (R_{\mathrm{A}} + R_{\nu}) \tag{4.23}$$

which in time makes

$$R_{\mathrm{tot}} = \frac{N_{\mathrm{L}}}{N_{\mathrm{p}}} (R_{\mathrm{A}} + R_{\nu}) . \tag{4.24}$$

Further

$$A_{p,tot} = \pi r_{\mathrm{p}}^2 N_{\mathrm{p}}$$

$$\implies N_{\mathrm{p}} = \frac{A_{p,tot}}{\pi r_{\mathrm{p}}^2} \tag{4.25}$$

where $A_{p,tot}$ is the total cross section area of all the anthracite particles. $A_{p,tot} = A_i(1 - \nu)$, where A_i is the total cross section area of volume i.

Similarly

$$h_{\mathrm{tot}} = (\beta r_{\mathrm{p}} + h_{\nu}) N_{\mathrm{L}}$$

$$N_{\mathrm{L}} = \frac{h_{\mathrm{tot}}}{\beta r_{\mathrm{p}} + h_{\nu}} \tag{4.26}$$

whit h_{tot} being the total height of the control volume. Inserting (4.21), (4.22), (4.25) and (4.26) into (4.24) gives

$$R_{\mathrm{tot}} = \frac{h_{\mathrm{tot}} \pi r_{\mathrm{p}}^2}{A_i(1 - \nu)(\beta r_{\mathrm{p}} + h_{\nu})} \left(\rho_{\mathrm{A}} \frac{\beta}{\pi r_{\mathrm{p}}} + \rho_{\nu} \frac{h_{\nu}}{\pi r_{\mathrm{p}}^2} \right) \tag{4.27}$$

The height of all the anthracite in the control volume h_{A} is given by

$$h_{\mathrm{A}} = \beta r_{\mathrm{p}} N_{\mathrm{L}} \tag{4.28}$$

and the height of all the void $h_{\mathrm{tot},\nu}$ by

$$h_{\mathrm{tot},\nu} = h_{\nu} N_{\mathrm{L}}. \tag{4.29}$$

The void fraction is how much percentage of void there is in the control volume, meaning that

$$\nu = \frac{h_{\mathrm{tot},\nu}}{h_{\mathrm{A}}} = \frac{h_{\nu} \cancel{N_{\mathrm{L}}}}{\beta r_{\mathrm{p}} \cancel{N_{\mathrm{L}}}} \tag{4.30}$$

$$\implies h_{\nu} = \nu \beta r_{\mathrm{p}} \tag{4.31}$$

Inserting (4.31) into (4.27) gives

$$\begin{aligned} R_{\text{tot}} &= \frac{h_{\text{tot}}\pi r_{\text{p}}^2}{A_i\left(1-\nu\right)\left(\beta r_{\text{p}}+\nu_\rho \beta r_{\text{p}}\right)}\left(\rho_{\text{A}}\frac{\beta}{\pi r_{\text{p}}}+\rho_\nu\frac{\nu\beta \cancel{r_{\text{p}}}}{\pi r_{\text{p}}^{\cancel{2}}}\right) \\ &= \frac{h_{\text{tot}}\cancel{\pi r_{\text{p}}^2}\beta}{A_i\left(1-\nu\right)\left(1+\nu\right)\cancel{\beta r_{\text{p}}}\cancel{\pi r_{\text{p}}}}\left(\rho_{\text{A}}+\rho_\nu\nu\right) \end{aligned}$$

and an expression for bulk resistance is found

$$R_{\text{bulk}}(\rho_{\text{A}},\nu) = R_{\text{tot}} = \frac{h_{\text{tot}}}{A_i\left(1-\nu^2\right)}\left(\rho_{\text{A}}+\rho_\nu\nu\right). \tag{4.32}$$

h_{tot}, A_i and ρ_ν is assumed constant, so the bulk resistance is only a function of the anthracite resistivity and the void fraction. This was what was desirable to find. It is not dependent on the particle size, or how the particles are stacked.

4.6 Heat transfer

The two dominating forms for heat transfer between control volumes is conduction and radiation. Radiation is dominating in the cavities between the material, and conduction is dominating when the material is in direct contact. Since plug flow is assumed the convection is disregarded between control volumes. A model is proposed for the relationship between radiation and conduction. Radiation from control volume i to j $Q_{r,i,j}$ is weighted by the void fraction ν [–], and conduction from i to j $Q_{c,i,j}$ with $1-\nu$

$$Q_{i,j} = \nu Q_{r,i,j} + (1-\nu)Q_{c,i,j}. \tag{4.33}$$

The radiation is found directly from Stefan-Boltzmann law

$$Q_{r,i,j} = \epsilon A_{i,j}\sigma(T_i^4 - T_j^4) \tag{4.34}$$

with $A_{i,j}$ being the cross section area between the two control volumes. ϵ is the emissivity, $\sigma = 5.67\times10^{-8}$ $[\mathrm{W}/(\mathrm{m}^2\,\mathrm{K}^4)]$ is the Stefan-Boltzmann constant, and T_i and T_j is the temperature of control volume i and j respectively.

The conduction heat between two control volumes can be computed as

$$Q_{c,i,j} = \frac{k_i}{l_{i,j}}A_{i,j}(T_i - T_{i,j}). \tag{4.35}$$

Here k_i $[\mathrm{W}/(\mathrm{m}\,\mathrm{K})]$ is the thermal conductivity of control volume i. $l_{i,j}$ $[\mathrm{m}]$ is the length from the middle of i to the interface between the control volumes, and $T_{i,j}$ is the temperature at said interface. $T_{i,j}$ can be found as

$$T_{i,j} = \frac{\frac{k_i}{l_{i,j}}T_i + \frac{k_j}{l_{j,i}}T_j}{\frac{k_i}{l_{i,j}} + \frac{k_j}{l_{j,i}}}. \tag{4.36}$$

Similarly the heat transfer to the electrodes are modelled as

$$Q_{i,el} = \frac{k_i}{l_{i,el}} A_{i,el}(T_i - T_{i,el}). \tag{4.37}$$

Here k_{el} is the electrodes thermal conductivity, $T_{i,el}$ is the temperature on the interface between the control volume and the electrode, and $l_{i,el}$ is the length from the middle of the control volume to the interface between them. $A_{i,el}$ is the cross section area between the electrode and the control volume.

Elkem Carbon (2016) gives a model for the heat flow through the furnace walls. It is assumed that this model is sufficiently good. As shown in Figure 4.10, the wall consist of four different substances. The green is a refractory lining, the blue is insulation bricks, the yellow is an insulation blanket, and the gray is a steel shell. It is seen that the temperature slope through the insulation bricks and the blanket is quite similar. To simplify the model, it is therefore said that yellow field is brick as well.

In Figure 4.10 the symbols T_1, T_2 and T_3 is used. These are symbols that are already used for something else in this report, and to avoid confusion the indexes 1, 2 and 4 will be replaced with l, b and s respectively. The layer corresponding to index 3 has been removed from the model, because the insulation bricks and the insulating blanket are assumed to be identical.

The heat transferred from control volume i out through the wall $Q_{i,0}$ is given by

$$Q_{i,0} = h_{wall} A_{i,w}(T_i - T_{wall}) \tag{4.38}$$

where

$$\begin{aligned} T_{wall} = &\frac{(\frac{k_s}{L_s}\frac{k_b}{L_b}\frac{k_l}{L_l}h_{wall} + h_{wall}\frac{k_l}{L_l}\frac{k_b}{L_b}h_{shell})T_i}{N} + \\ &\frac{(h_{wall}\frac{k_l}{L_l}\frac{k_s}{L_s}h_{shell} + h_{wall}\frac{k_b}{L_b}\frac{k_s}{L_s}h_{shell})T_i + \frac{k_l}{L_l}\frac{k_b}{L_b}\frac{k_s}{L_s}h_{shell}T_0}{N}. \end{aligned} \tag{4.39}$$

$$\begin{aligned} N = &\frac{k_s}{L_s}\frac{k_b}{L_b}\frac{k_l}{L_l}h_{wall} + h_{wall}\frac{k_l}{L_l}\frac{k_b}{L_b}h_{shell} + h_{wall}\frac{k_l}{L_l}\frac{k_s}{L_s}h_{shell} \\ &+h_{wall}\frac{k_b}{L_b}\frac{k_s}{L_s}h_{shell} + \frac{k_l}{L_l}\frac{k_b}{L_b}\frac{k_s}{L_s}h_{shell}. \end{aligned} \tag{4.40}$$

The symbols used in (4.38)-(4.40) are explained in Table 4.2.

In the model for the heat transfer through the wall, steady state is assumed. In reality the wall, and especially the thick refractory lining, would contribute to the heat capacity of the system, and in turn the dominating time constant. This would make the assumption a bad one. The argument for the assumption is that the temperature differences under normal operations will be relative small, and these contributions from the wall might be negligible. However, this argument might not be sufficient, and the model for the heat transfer through the wall is probably one of the weak points of the model over all. In further works a more dynamic model for the heat transfer through the wall should be developed.

Table 4.2: Symbol explanation of (4.38)-(4.40).

Symbol	Unit	Explanation
$Q_{i,0}$	W	Heat from control volume i out through the wall
T_i	K	Temperature in control volume i
T_{wall}	K	Temperature at the inner edge of the wall
$A_{i,w}$	m^2	Cross section area between control volume and wall
h_{wall}	$\mathrm{W}/(\mathrm{m}^2\,\mathrm{K})$	Convection coefficient between anthracite and wall
h_{shell}	$\mathrm{W}/(\mathrm{m}^2\,\mathrm{K})$	Convection coefficient between steel shell and air
k_l	$\mathrm{W}/(\mathrm{m}\,\mathrm{K})$	Thermal conductivity of refractory lining
k_b	$\mathrm{W}/(\mathrm{m}\,\mathrm{K})$	Thermal conductivity of insulation bricks
k_s	$\mathrm{W}/(\mathrm{m}\,\mathrm{K})$	Thermal conductivity of steel shell
L_l	m	Length of refractory lining in x-direction
L_b	m	Length of insulation bricks in x-direction
L_s	m	Length of steel shell in x-direction

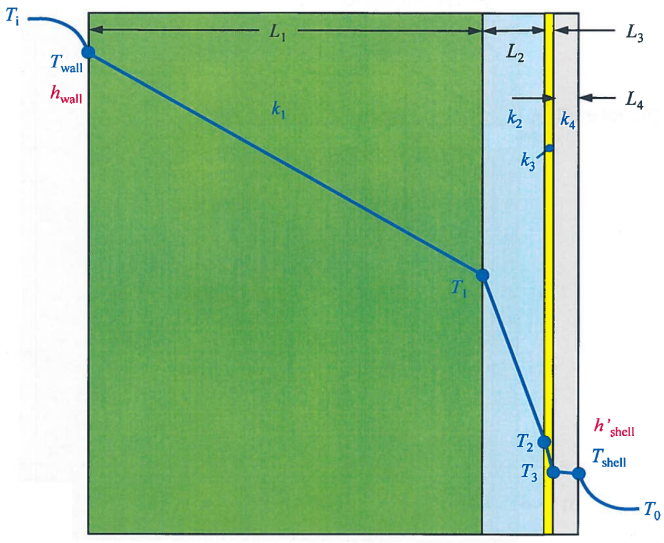

Figure 4.10: Temperature profile through the wall. From Elkem Carbon (2016).

4.7 Parameter estimation

Maybe the greatest challenge in the model development is finding numerical values for all the parameters. There are a lot of parameters in the model. Many of the parameters are hard to find theoretical values for, and many are very dependent on the raw material that are used.

Ideally, extensive analysis on the raw material to find the best parameter values should be done. That was unfortunately not possible in conjunction with this work. Instead many parameter values had to be guessed at or estimated to get the best fit of the model.

A lot of the parameters are coupled or are parameters on nonlinear effects. This have to be considered when estimating the parameters. Some parameter estimation tools where used (mainly Cybernetica ModelFit), but most of the parameters where find manually through trial and error. This took up a large part of the labor done on this work.

The numerical values for the parameters used in the final model is given in Appendix A.

Chapter 5

Model validation

In an attempt to validate the model it is compared with measurements provided by Elkem Carbon. These measurements are from a calcination furnace under normal operation. The inputs used are also provided. The measurements are strictly confidential. The data is therefore anonymized.

Elkem has provided two data series. The first is from a one-week period, and the second from a two-week period about 20 weeks later; both are from 2016. The model is simulated using Cybernetica ModelFit.

The resistivity that is measured is a specific resistivity for the finished product. The resistance that is measured is the furnace's operation resistance.

5.1 Voltage and current comparison

The best obtained results for the resistance and resistivity for the one-week period is shown in Figure 5.1, and for the two-week period in Figure 5.2. The different results are not found using the same parameter values. This because when voltage is used as input, and the parameters that yields best current results applied, thermal runaway is present in the model. Then the comparison is not of any interest. It is more interesting to see how good of a match it is possible to get with the respective inputs.

It was not possible to make the modelled dynamic of the resistance match the measured resistance when using the voltage as input. However, there appears to be some high frequency variations on the resistance measurements. These measurements was filtered by a Savitzky-Golay filter, which is described in detail in Savitzky and Golay (1964), to examine if the variations might be caused by measurement noise. It was interesting to see if it was possible to get a better fit with filtered measurements. Parameter estimation tools where then used to try to make the modeled curve fit the filtered curve as good as possible. The results of this is seen in Figure 5.1a and Figure 5.2a. In the one-week period the model fitted the filtered resistance fairly well. In the two-week period however, the best achieved curve does not match the dynamic in a satisfactory manner when using voltage as input.

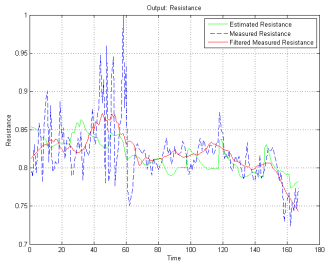

(a) Best resistance results using voltage as input.

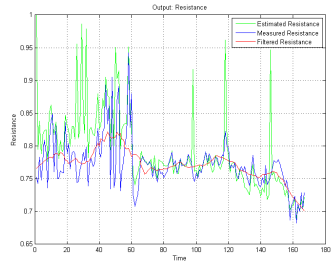

(b) Best resistance results using current as input.

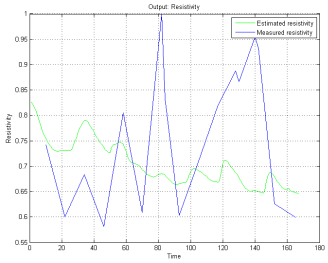

(c) Best resistivity results using voltage as input.

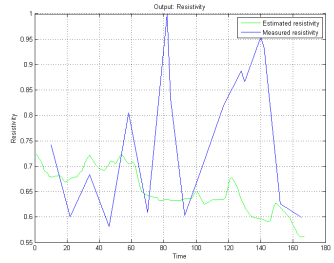

(d) Best resistivity results using current as input.

Figure 5.1: Comparison of results with voltage and current as input for a one-week period.

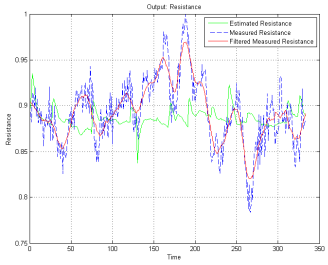

(a) Best resistance results using voltage as input.

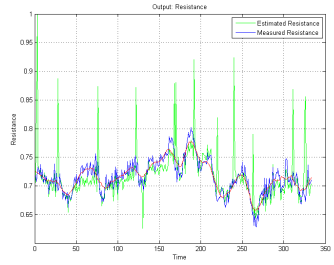

(b) Best resistance results using current as input.

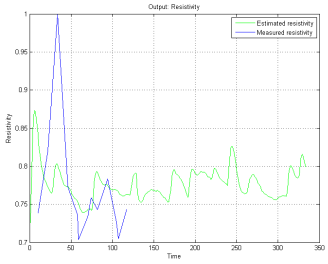

(c) Best resistivity results using voltage as input.

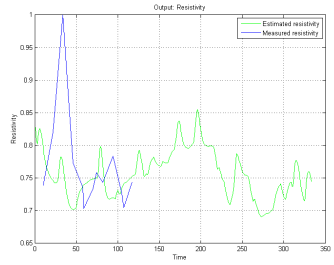

(d) Best resistivity results using current as input.

Figure 5.2: Comparison of results with voltage and current as input for a two-week period.

Compared to the resistance when current is used as input, shown in Figure 5.1b and Figure 5.2b, it is easy to see that the current yields better results. Here the dynamics of the modelled and measured resistance match very well, except some spikes and the start of the one-week period. The model picks up the dynamics in the actual resistance measurement, not the filtered one. It is more likely that the high frequency variations in the resistance is caused by high frequency variations in the input, rather than measurement noise. It is therefore better to match the non-filtered measurements.

When using the same parameters with voltage as input as the best fit current curve, thermal runaway is introduced. This might be the reason why it is not possible to make the resistance match while using voltage input.

There isn't that much of a difference between the resistivity results, and none of them are a great fit, but the ones with current as input is arguably a little better. Since the resistance results are that much better, the current is used as input for the rest of this work.

5.2 Activation energy

In section 4.2 it is speculated that a lower effective activation energy than the one used in Wilson (2016) will lead to a more dynamic resistivity curve. In this section it is examined if this is the case.

Figure 5.3 show resistivity curves with different effective activation energy and reaction rate constants. All other parameters are kept the constant for all the curves. The effective activation energy and the reaction rate are strongly coupled, and it is not meaningful to change one without changing the other.

The parameters used for the green curve is the ones that are used in Wilson (2016): $E = 960$ [kJ/mol] and $n = 1 \implies Q = 960$ [kJ/mol]. The parameters used for the magenta curve is based on Brandtzæg et al. (2016): $E = 340$ [kJ/mol] and $n = 0.087 \implies Q = 29.58$ [kJ/mol]. The parameters for the red curve is the result of tuning: $E = 340$ [kJ/mol] and $n = 0.3059 \implies Q = 104$ [kJ/mol]. Alternatively $E = 960$ [kJ/mol] and $n = 0.1083 \implies Q = 104$ [kJ/mol].

By comparing the green curve to the two other curves, it is evident that it is possible to get a more dynamic resistivity curve than the one found in Wilson (2016). This is caused by lowering the effective activation energy. While the effective activation energy is as high as $Q = 960$ [kJ/mol], it is not possible to achieve a smooth dynamic of the resistivity curve. If the reaction rate constant is chosen really high (for example $k = 10^{21}$) it is possible to achieve oscillation, but not to get a smooth dynamic.

However, it is not possible to conclude that lower effective activation energy leads to a more dynamic resistivity curve in general. The red curve has a higher effective activation energy than the magenta one, but also has more dynamics. It is hard to separate the contribution from the effective activation energy and the reaction rate constant in this case.

The important conclusion to draw from this is that it is possible to achieve a more dynamic resistivity curve than the one used in Wilson (2016). This was also what was speculated to be the case in section 4.2.

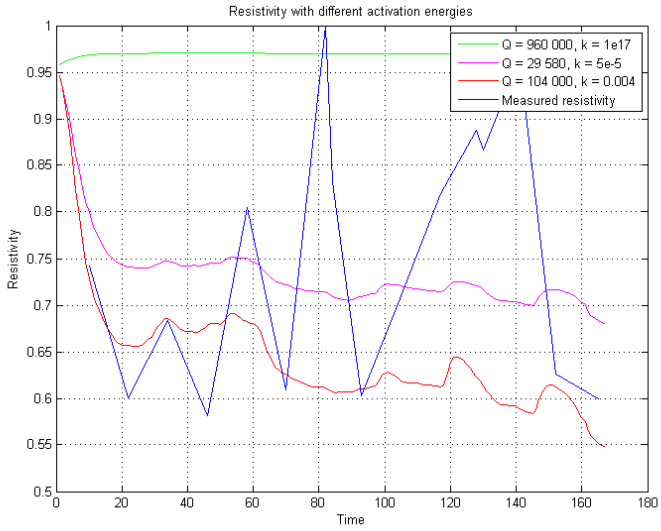

Figure 5.3: Comparisons of different resistivity curves using different effective activation energies and reaction rate constants.

5.3 Simulation results

Simulations of the furnace for the two periods were run. The parameters where chosen to try to make the model match all the measurements at once. The inputs to the one-week period are shown in Figure 5.4. The given outputs with model estimation are plotted in Figure 5.5. The inputs and outputs to the two-week period are given respectively in Figure 5.6 and Figure 5.7. The same parameters are used for all the curves, and for both periods.

5.4 Discussion

From the simulation results presented in Section 5.3 it is seen that the estimated voltage and power matches the measured values well. The match between estimated and measured resistance is not that bad. The estimated and measured resistivity however, does not match that well.

It is hard to see any direct correlation between the inputs and the resistivity output. This might suggest that there are factors other than the inputs alone, that determine the resistivity of the finished product. Such a factor could be differences in the raw material.

Differences in raw material properties can be caused by different moisture and volatile fractions, differences in natural occurring graphite, and variations in heat capacity and thermal conductivity. The raw material property most likely to influence the resistivity of the finished product is probably the numbers of cross links between layers in the carbon structure.

As discussed in Section 2.1.3, there are great differences in graphitization of anthracite

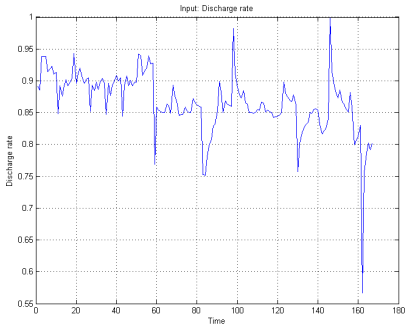

(a) Discharge rate

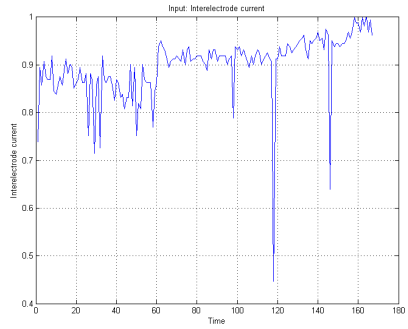

(b) Interelectrode current

Figure 5.4: Input to the furnace in the one-week period.

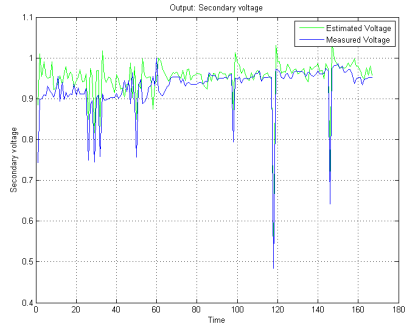

(a) Secondary voltage

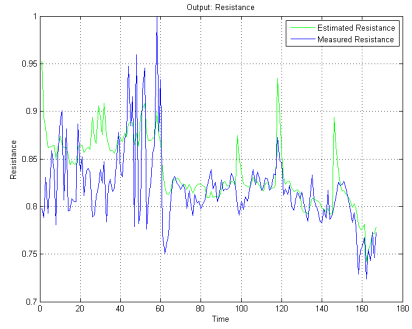

(b) Furnace resistance

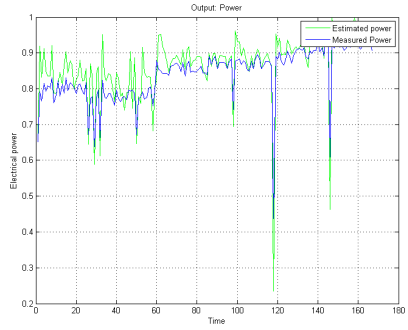

(c) Electrical power in the furnace

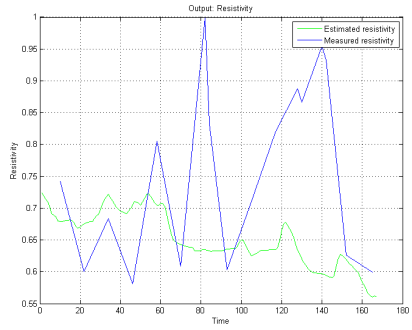

(d) Resistivity of finished product

Figure 5.5: Output of the furnace in the one-week period.

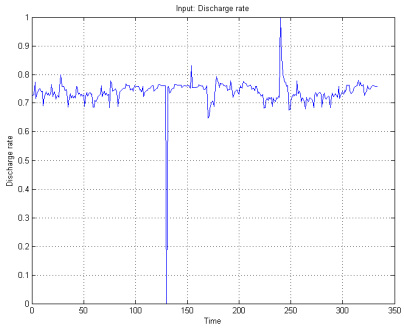

(a) Discharge rate

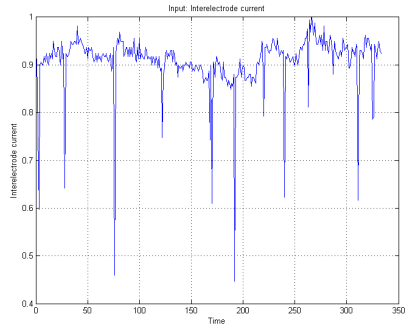

(b) Interelectrode current

Figure 5.6: Input to the furnace in the two-week period.

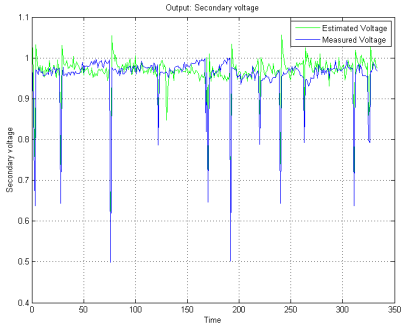

(a) Secondary voltage

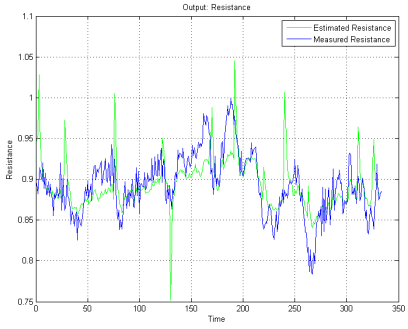

(b) Furnace resistance

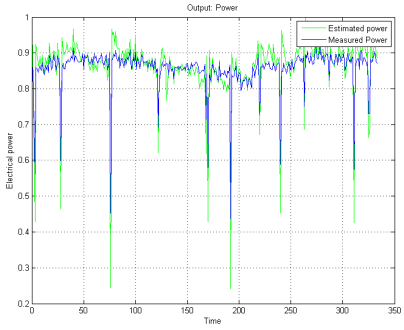

(c) Electrical power in the furnace

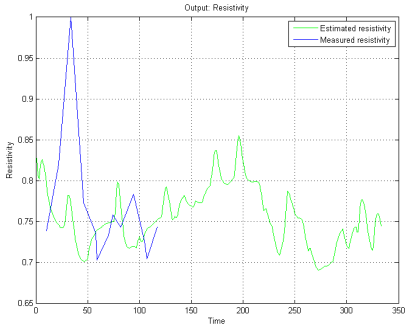

(d) Resistivity of finished product

Figure 5.7: Output of the furnace in the two-week period.

dependent on these cross links. This could explain the great changes in the finished resistivity, that seem independent of the inputs. In further works, experiments to determine what effect the microstructur of the carbon has on the finished product resistivity should be conducted.

There isn't any obvious correlation between the measured resistance and the measured resistivity. This is odd because the resistivity should directly determine the resistance in the furnace. When comparing the estimated resistivity and the estimated resistance it is a clear correlation in the dynamics. It is obvious that this is the case when regarding the equations for the electrical system. One reason why there isn't any correlation between the measured resistance and resistivity might be that the resistivity measurements are poor.

Since the measured resistivity isn't correlated with neither the inputs nor the rest of the measurements in the furnace, it is assumed that these measurements can not be trusted. These measurements are therefore disregarded. Elkem Carbon (2017) confirms that the sampling and analyzing of the finished product's resistivity is very uncertain. The furnace resistance is therefore used for validation purposes instead.

The resistance is directly computed from the resistivity. This means that if the correct resistivity distribution is given, it is easy to compute the correct resistance in each control volume, which again should yield the correct furnace resistance, if the model is correct. If the correct furnace resistance is given however, it is not necessarily possible to find the correct resistivity distribution, since there will be many distributions that yields the same furnace resistance. For instance, all three resistivity curves in 5.3 gives a good resistance match. This means that the model in practice can not be validated before trustworthy resistivity measurements are obtained.

For the purpose of this work, it is assumed that the model is satisfactory as it is now. This to be able to suggest a controller and see how it behaves. In further works there should be efforts to find more trustworthy resistivity measurement to validate the model against.

Chapter 6

Controller

The ultimate goal of the work on the electro calciner is to find a controller that yields consistent resistivity of the finished calcined carbon. It is thought that an MPC controller would be able to achieve the desired result. The MPC basics are given in Section 2.4. In this chapter the control scheme will be described, then two control cases will be presented.

The model is highly nonlinear. One example of a nonlinearity is the resistivity's reaction rate given in (4.4) as

$$s_i = (\rho_i - \rho_s(T, \text{type}))k_\rho e^{\frac{-nE}{RT}}.$$

Other examples are the radiation $Q_{r,i,j} = \epsilon A_{i,j}\sigma(T_i^4 - T_j^4)$ and the ohmic heating $P_{el,i} = R_i I_i^2$. This means that an NMPC controller will be used.

To relate the model to the MPC notation used in Section 2.4, the model should be written in the general form

$$\dot{\mathbf{x}} = f(\mathbf{x}, \mathbf{u}). \tag{6.1}$$

6.1 Model on general form

The input vector $\mathbf{u} \in \mathbb{R}^2$ is

$$\mathbf{u} = \begin{bmatrix} w_{out} \\ I_s \end{bmatrix} \tag{6.2}$$

and the model's state vector $\mathbf{x} \in \mathbb{R}^{36}$ is given as

$$\mathbf{x} = \begin{bmatrix} m_1 \\ m_2 \\ \vdots \\ m_{12} \\ \rho_1 \\ \rho_2 \\ \vdots \\ \rho_{12} \\ T_1 \\ T_2 \\ \vdots \\ T_{12} \end{bmatrix}. \tag{6.3}$$

The nonlinear function $f(\mathbf{x}, \mathbf{u})$ is

$$f(\mathbf{x}, \mathbf{u}) = \begin{bmatrix} (4.2) \\ (4.7) \\ (4.9) \end{bmatrix}. \tag{6.4}$$

Finally the output $z \in \mathbb{R}$ is

$$z = \rho_{out} \tag{6.5}$$

with corresponding measurement function

$$z = g(\mathbf{x}) = \frac{w_{out,5}\rho_5 + w_{out,10}\rho_{10}}{w_{out,5} + w_{out,10}}. \tag{6.6}$$

6.2 Control formulation

The NMPC formulation for the calcination controller can be written as

$$\begin{aligned}
\min_{\xi} h(\xi) = \sum_{k=0}^{N-1} & \frac{1}{2} q_{k+1} (\rho_{ref,k+1} - \rho_{out,k+1})^2 + \frac{1}{2} \mathbf{u}_k^{\mathrm{T}} \boldsymbol{R}_k \mathbf{u}_k \\
& + \frac{1}{2} \boldsymbol{\Delta}\mathbf{u}_k^{\mathrm{T}} \boldsymbol{S}_k \boldsymbol{\Delta}\mathbf{u}_k + \frac{1}{2} p_{q,k} \varepsilon_k^2 + p_{l,k} \varepsilon_k && \text{(6.7a)} \\
\text{s.t.} \quad \mathbf{x}_{k+1} &= f(\mathbf{x}_k, \mathbf{u}_k) && \text{(6.7b)} \\
\rho_{min} - \varepsilon_k &\leq \rho_k \leq \rho_{max} + \varepsilon_k && \text{(6.7c)} \\
0 &\leq \varepsilon_k \leq \varepsilon_{max} && \text{(6.7d)} \\
\mathbf{u}_{min} &\leq \mathbf{u}_k \leq \mathbf{u}_{max} && \text{(6.7e)} \\
\boldsymbol{\Delta}\mathbf{u}_{min} &\leq \boldsymbol{\Delta}\mathbf{u}_k \leq \boldsymbol{\Delta}\mathbf{u}_{max} && \text{(6.7f)} \\
\rho_{out,0}, &\quad \text{given} && \text{(6.7g)}
\end{aligned}$$

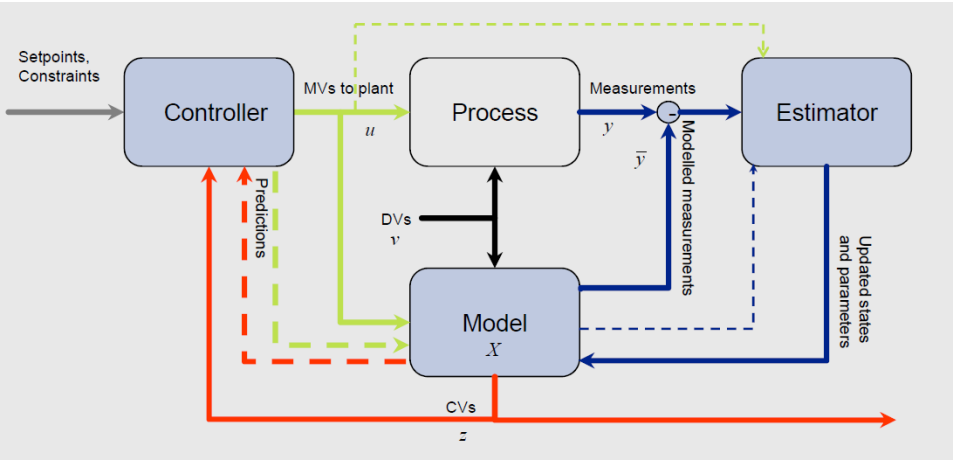

Figure 6.1: The closed loop control system. From Dyrset and Hauger (2015).

Assuming that the model is sufficiently good, and there is enough knowledge of the disturbances, this controller should be able control the resistivity to the desired reference ρ_{ref} given the right tuning. Since the output is a scalar, the matrices $\boldsymbol{Q}_{k+1}$ and $\boldsymbol{P}_k$, and the vector $\mathbf{p}_k$, are reduced to scalars. $p_{q,k}$ are used to penalize the quadratic cost of the slack variable, while $p_{l,k}$ are used to penalize the linear cost.

The closed loop control system is given in 6.1. The estimator is not used in this implementation, but is included in the figure because it is a part of the Cybernetica CENIT software.

6.3 Control cases

Two cases will be simulated to observe the controllers behaviour. In both cases the model developed in this work will be used both as the control model, and the plant model. The plant model means the model used to simulate the plant, and the control model is the one used by the controller. There are some benefits in having different models for the controller and the plant. In real life there will always be some difference between the controller model and the plant. Using different models for the two will better show the controllers robustness if it is still able to achieve satisfactory control.

Since the control model and the plant model is identical, the process measurement y and the modelled measurement $\hat{y}$ shown in Figure 6.1 will be identical as well. This means that the estimator will be inactive.

In this work, no separate model for the plant is developed. Simulations will still be useful to show the controller's principal behaviour. However, a separate plant model would probably be useful, and should be developed in further works.

6.3.1 Control case I: Change of resistivity set point

This first case is the base case: **Steady control of resistivity when there are no model deviations or disturbances.**

In this case the controller will first need to control the resistivity from the initial value to the initial set point. Afterwards the set point will be changed two times, once to a higher value than the initial set point, and once to a lower value. It will be studied how the controller behaves in these different situations.

6.3.2 Control case II: Differences in raw material's moisture

The second case is: **Steady control of resistivity when there are differences in the raw material's moisture.**

Elkem has stated that this case is of great interest for their operation.

In this case the difference in moisture will modeled as a disturbance. It is assumed that that the moisture is measured. The moisture will then be used as a feed-forward. The assumption that the moisture is measured is a reasonable one. The moisture is often analyzed in raw materials. A natural way of doing this would be to measure the raw material's moisture upon delivery. Each delivery of raw material should be stored separately and dry. How representative the measurements are for the raw material most be considered in a real implementation.

The resistivity set point will be held constant for this case. There will only be a change in the raw material's moisture content.

6.4 Controller tuning

The controller is tuned through trial and error, in combination with educated guess using process knowledge. In this work all penalty parameters and matrices are constant for all time steps, meaning that $q_k = q_{k+1} = q$, $\boldsymbol{R}_k = \boldsymbol{R}_{k+1} = \boldsymbol{R}$ and so on.

The final tuning used for all simulation of the controller in this work is

$$q = 1 \tag{6.8a}$$

$$\boldsymbol{R} = \begin{bmatrix} 0 & 0 \\ 0 & 0 \end{bmatrix} \tag{6.8b}$$

$$\boldsymbol{S} = \begin{bmatrix} 0.5 & 0 \\ 0 & 0.1 \end{bmatrix}. \tag{6.8c}$$

With this tuning, the deviation from the resistivity set point is penalized most. The change in discharge rate is penalized more than the change in current. This seems reasonable because the current can be changed rather rapidly, while the change in discharge rate is mechanical which makes it slower. It should be examined closer if these penalties reflects the physical properties of the process.

Minimizing the input is just a bonus; the resistivity control is the main objective. Penalizing the input in a significant way lead to unsatisfactory control of the resistivity. References for the inputs that yields stationary correct resistivity values need to be used or

else the minimizing of the inputs will be at the expense of the resistivity control. These input references were not known. Therefore it was decided to not penalize the absolute value of the input at all.

The prediction horizon should be chosen larger than the process' dominant time constant, which is said to be around 12 hours. Therefore the prediction horizon is chosen as $N = 14$ [h].

No stability problems were observed with any of the tunings that were tested.

Chapter 7

Results and Discussion

In this chapter the simulation results of the two cases introduced in Section 6.3 will be presented. The results will be discussed in the same section that they are presented.

All data are anonymized. This is done to not give away any sensitive data about Elkem's region of operation. The value of the output and inputs are blue, the set point is dotted green, and the constraints are dotted red.

7.1 Control case I: Change of resistivity set point

The results of simulating case I is given in Figure 7.1. As described in Section 6.3 the set point start at an initial value, and gets changed two times.

Here the initial set point is 0.5 of this scale, while the initial resistivity is 0.7272. When the controller reached the set point, the set point was change to 0.7. After this set point was reached, the set point was change again, this time to 0.35.

It was observed that the controller was able to reach and hold the desired set points.

As a whole it was observed that the controller gives smooth and satisfactory control of the finished resistivity for this case, with the given set points and set point changes.

In this case there is no disturbances or model deviations, this is not possible in a real process. It is therefore not possible to conclude that the controller will work satisfactory in the real process based on this result. However, this is the natural starting point for validation of the controller. If the controller wasn't able to get satisfactory results in this easy case, it could safely be dismissed.

Since the controller worked satisfactory, there is no need to dismiss the controller yet, and further work on validation can be done. The natural next step would be to test the controller while using a different model for the plant and the controller, which will further test the controller's robustness. This will not be done in this work. It can however, easily be implemented by changing some of the model parameters.

Ultimately the controller must be implemented on the plant to make conclusions on how well it works in practice.

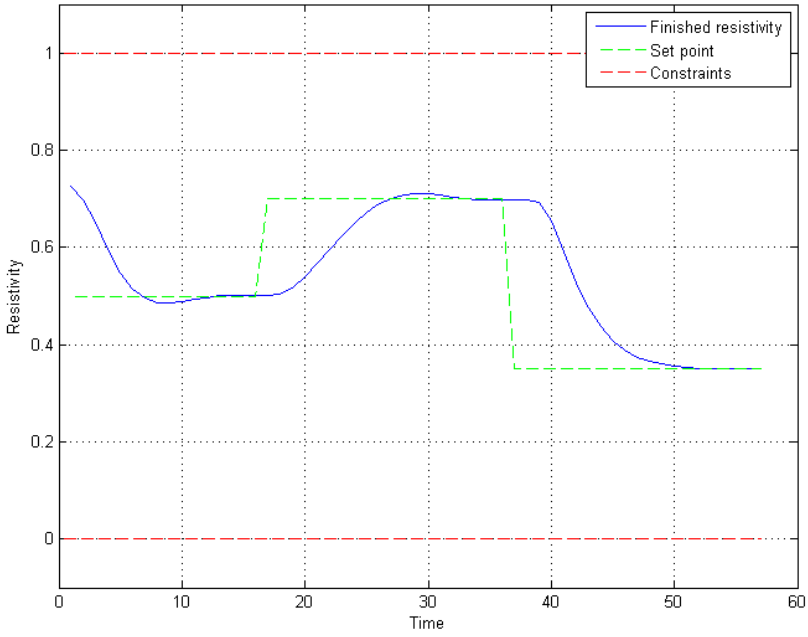

(a) Output: Finished resistivity

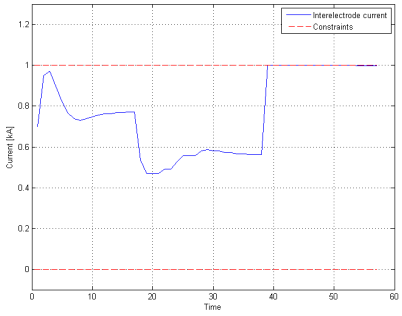

(b) Input: Current.

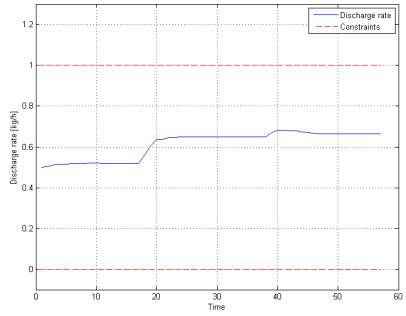

(c) Input: Discharge rate

Figure 7.1: Results of simulating Case I.

7.2 Control case II: Differences in raw material's moisture

This case starts with steady control of the resistivity when the set point is 0.5. At time $\tau = 0$ the moisture content in the anthracite is change from 8% to 40%. Weight percentage is used implicitly in the whole section. There is no set point change in this case.

The moisture is only included in the model through the energy balance, and only as the energy needed to vaporize the water. The parts of the equations in question is

$$-\Delta H_{R_{\mathrm{H_2O}}} X_{\mathrm{H_2O},1} w_{in,1}$$

from (4.9a), and

$$-\Delta H_{R_{\mathrm{H_2O}}} X_{\mathrm{H_2O},6} w_{in,6}$$

from (4.9f). This means that if the moisture increases the temperature in control volume 1 and 6 will decrease. This will in turn make the temperature in all the other control volumes decrease. When the temperature decreases there is less graphitization and the resistivity increases.

It turns out that the moisture content in the raw material doesn't effect the numerical values of the model in a significant manner. This might be a weak point in the model. The significance of moisture content in the raw material should be examined closer in further works. If the model is representative of the plant with regards to the moisture content, there would not in practice be any point of introducing feed-forward using the moisture measurements. Other disturbances, e.g. uneven granular flow or unsymmetrical current paths, and model deviations would have a much larger numerical effect than the moisture content in this case.

The case is still included in this work. The reason for this is even though the numerical values is insignificant, it shows the conceptual benefits of the control scheme. It is reasonably to assume that these would apply also with larger numerical values.

As stated in the start of this section, the moisture content is change from 8% to 40%. This is an unrealistically large change in moisture content, or said in another way: 40% moisture content for anthracite is unrealistically high. The moisture content of anthracite will probably never exceed 20%. 40% is used nevertheless to get larger deviations. If the controller is able to handle the more extreme case, it should be able to handle the simpler case.

The results of simulating case II is given in 7.2. The case without feed-forward is seen in Figure 7.2a and is included as a comparison. This will be called the base case. The case simulated with feed-forward and the same scale on the axis as Figure 7.2a for easy comparison is given in 7.2b. Figure 7.2c is the same plot as Figure 7.2b only zoomed into the most relevant part.

The controller is not able to obtain the set point when the moisture is changed without feed-forward, it gets a stationary deviation. Here there will be a difference between the plant model and the control model, and the controller is not able to overcome this.

When there is feed-forward in the controller, it is able to reach the set point. The controller is smooth, and quite fast. The deviation form the set point before the set point

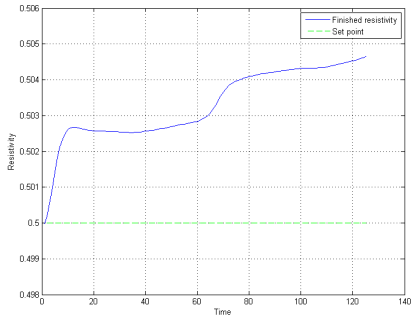

(a) Resistivity without feed-forward.

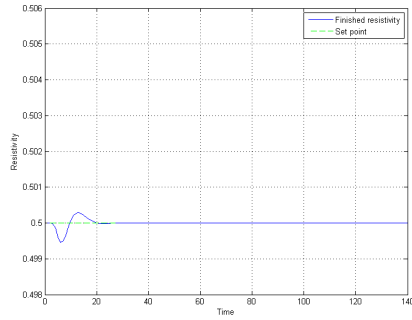

(b) Resistivty with feed-forward with same scale.

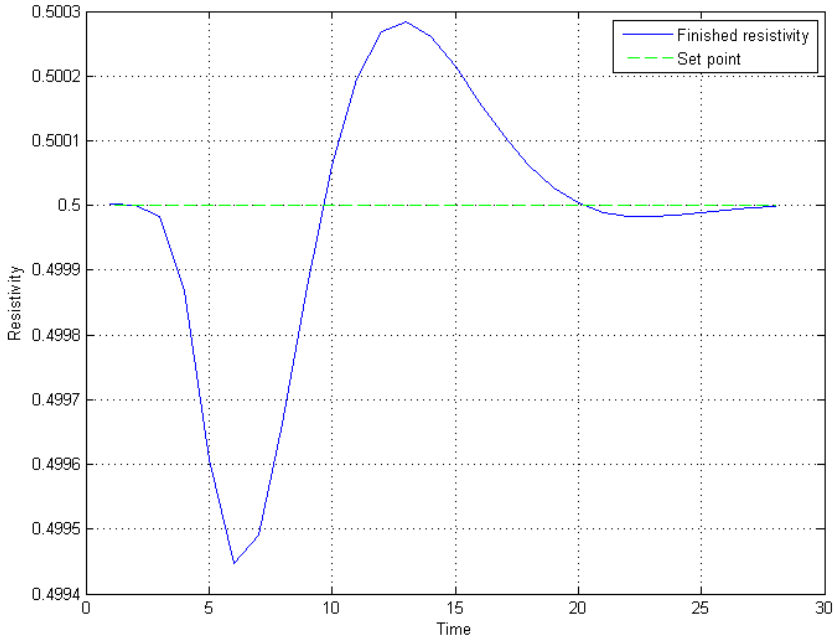

(c) Resistivty with feed-forward zoomed.

Figure 7.2: Results of simulating Case II.

is reached is very small compered to the deviation in the base case. In conclusion: this control scheme was successful, at least in theory.

If it is not possible to get moisture measurements of the raw material, feed-forward can not be used. Then some sort of integral action probably needs to be introduced. For the feed-forward scheme to work as well as presented here, the model must be a perfect representation of the plant, which will never be the case. Therefore there would be desirable with some integral action in any case. The integral action will also help counteract unmeasured disturbances. In further works, integral action should be introduced to the controller.

Chapter 8

Conclusion

The purpose of this work was to develop a mathematical model for the electric calcination of anthracite process, and then propose a control scheme for consistent control of the finished anthracite's electrical resistivity.

The model is developed using first principles. The model is then simulated and compared to real operational data from normal operation of the process. The voltage and current are both used as input, and the results from the different inputs are compared. It is concluded that using current as an input yields much better match between the measured and modelled values, compared to when the voltage is used as input. This might be because thermal runaway is introduced into the model when voltage is used, when there is no indication that this is present in the normal operation range.

It is shown that the effective activation energy combined with the reaction rate constant has a great effect on the dynamics of the finished resistivity. By choosing an effective activation energy that is lower than the one used in Wilson (2016) ($Q = 960$ [kJ/mol]), it is possible to get a more dynamic resistivity curve. It is however not found any general rule on the effective activation energy behaviour. The effective activation energy is strongly coupled with the reaction rate constant, and it is hard to say anything about these parameters behaviours separately.

By choosing the right parameters it is possible to get a good match between the model and the measurements for all the electrical properties, except the finished resistivity. This combined with the fact that there doesn't seem to be any direct correlation between the input measurements and the output (resistivity) measurements, leads to questioning the validity of the resistivity measurements. It is concluded that these measurements might not be trustworthy. This later gets confirmed by Elkem. The resistivity measurements are therefore dismissed, and not used in validating the model.

The model is validated using the furnace resistance, where there is a good match. The resistance is a direct result of the resistivity, meaning that if the resistivity is correct, the resistance also gets correct. However, the reverse is unfortunately not true. There is possible to have a lot of different resistivity distributions in the furnace that yields the same furnace resistance. The finished resistivity might also differ a lot. It is concluded

that the model can not be truly verified before trustworthy measurements of the resistivity is obtained.

The model is nevertheless deemed good enough to use as a model in a model based control scheme in this work.

A NMPC controller is suggested for the process. The controller yields satisfactory control of the finished anthracite's electrical resistivity, when the same model is used for both simulating the plant and in the controller. At least when there are no disturbances or model deviations. No conclusion can be made on the controller's behaviour on the real plant based on this, but it is an important first step in validating the controller.

The controller is tested on a case where the moisture content in the raw material is abruptly changed. The controller is not able to reach the set point when this change is unknown to the controller. When the moisture content is measured and feed-forwarded however, smooth and satisfactory control is achieved. The set point now get reached.

8.1 Further work

There is a lot that can be done in further works on this subject. This are brought up in discussions previous in this work. They will be summarized here.

In section 1.6 it is said that the main challenge in achieving efficient control lies in finding a satisfactory model. A lot of effort should be made in improving and validating the model. The most important thing would be to find trustworthy measurements of the finished product resistivity, preferably with a much higher sample rate than currently provided. This is a crucial step in validating the model, and the modelled resistivity dynamics.

A study on the effect differences in raw materials have on calcination properties should be conducted. Which properties is most significant:

- Moisture content?
- Volatile content?
- Natural occurring graphite content?
- Variations in heat capacity?
- Variations in thermal conductivity?
- Number of cross links between layers in the carbon structure?
- Other properties?

How is these differences in properties manifested in the calcination process? Answers to these questions will not only be useful for this work. It will give a greater understanding of the ECA process and of anthracite as a material.

Some of the weak points of the model is thought to be that a steady state model is used for the heat transfer through the wall, and the small significance the moisture content has on the model. A more dynamic model should be developed for the heat transfer. The actual significance the moisture content has on the process should be examined. This can

be combined with the study suggested above, or it can be examined in of itself. If results is found that significantly changes the moisture content's role in the model, control case II should be done over again for the new results. It would be interesting to see if the results were principally the same, or if the results differ greatly.

If it turns out that it is not possible or practical to measure the moisture content of the raw material, and it is found that the moisture content is significant for the end result, some other solution should be suggested. Integral action should be introduced to the controller.

It is concluded that no conclusion can be drawn regarding the controller behaviour if implemented on the plant. Further work should be done on validating the controller. As mentioned in section 7.1, the next step could be to examine how well the controller manages model deviations. A separate plant model should be developed, and an estimator should be designed.

The motivation for this work is to get consistent control of the finished ECA's resistivity. The final validation of the controller has to be done on the plant itself. This should be done after the model and the controller is deemed satisfactory through simulations.

Bibliography

Andrésen, J. M., Burgess, C. E., Pappano, P. J., Schobert, H. H., 2004. New directions for non-fuel uses of anthracites. Fuel processing technology 85 (12), 1373–1392.

Aylward, G. H., Findlay, T. J. V. a., 2008. SI chemical data, 6th Edition. New York, Wiley.

Belitskus, D., 1977. Effects of anthracite calcination and formulation variables on properties of bench scale aluminum smelting cell cathodes. Metallurgical Transactions B 8 (4), 591–596.

Bergman, T. L., Incropera, F. P., DeWitt, D. P., Lavine, A. S., 2011. Fundamentals of heat and mass transfer. John Wiley & Sons.

Bossel, U., 2003. Well-to-wheel studies, heating values, and the energy conservation principle. In: European Fuel Cell Forum. Vol. 22.

Bowen, B., Irwin, M., 2008. Coal characteristics. CCTR Basic Facts File 8.

Box, G. E., 1976. Science and statistics. Journal of the American Statistical Association 71 (356), 791–799.

Box, G. E., 1979. Robustness in the strategy of scientific model building. Robustness in statistics 1, 201–236.

Brandtzæg, S., Linga, H., Øye, H., 2016. Structural changes in carbon by heat treatment. In: Essential Readings in Light Metals. Springer, pp. 754–761.

Brandtzæg, S. R., 1985. Structural changes during calcination of coke and anthracite. Institutt for uorganisk kjemi, Norges tekniske høgskole, Universitetet i Trondheim.

Budd, C., Chapman, S., King, J., Lacey, A., Larson, D., Peletier, M., Please, C., Riley, D., Wheeler, A., Wood, G., 1995. Temperature variations and control of a calciner.

Burgess-Clifford, C. E., Narayanan, D. L., Van Essendelft, D. T., Jain, P., Sakti, A., Lueking, A. D., 2009. The effect of calcination on reactive milling of anthracite as potential precursor for graphite production. Fuel Processing Technology 90 (12), 1515–1523.

Cagienard, R., Grieder, P., Kerrigan, E. C., Morari, M., 2007. Move blocking strategies in receding horizon control. Journal of Process Control 17 (6), 563–570.

Cybernetica, 2017. Home page.
URL http://cybernetica.no/

Dyrset, J. G., Hauger, S. O., 2015. Recoba - training event. Confidential.

Edwards, I. A., Menendez, R., Marsh, H., 2013. Introduction to carbon science. Butterworth-Heinemann.

Elkem Carbon, 2016. Steady-state heat flow. Confidential.

Elkem Carbon, 2017. Personal communication. Confidential.

Engineering Toolbox, T., 2016a. Fluids - latent heat of evaporation.
URL http://www.engineeringtoolbox.com/fluids-evaporation-latent-heat-d_147.html

Engineering Toolbox, T., 2016b. Solids - specific heats.
URL http://www.engineeringtoolbox.com/specific-heat-solids-d_154.html

Findeisen, R., Imsland, L., Allgower, F., Foss, B. A., 2003. State and output feedback nonlinear model predictive control: An overview. European journal of control 9 (2-3), 190–206.

Fletcher, T., Baxter, L., Ottesen, D., 1988. Spectral emission characteristics of size-graded coal particles. Prepr. Pap., Am. Chem. Soc., Div. Fuel Chem.;(United States) 32 (CONF-870802-).

Foss, B., Heirung, T. A. N., 2013. Merging optimization and control. Lecture Notes.

Gasik, M., Gasik, M., Urazlina, O. Y., Kutuzov, S., 2010. Modelling and optimisation of anthracite treatment in an electrocalcinator.

Gundersen, O., 1998. Modelling of structure and properties of soft carbons with application to carbon anode baking. Ph.D. thesis, NTNU.

Hindmarsh, A., Serban, R., 2004. User Documentation for CVODES v2. 1.0. United States. Department of Energy.

Hovd, M., Braatz, R. D., 2001. Handling state and output constraints in mpc using time-dependent weights. In: American Control Conference, 2001. Proceedings of the 2001. Vol. 3. IEEE, pp. 2418–2423.

Hovd, M., Stoican, F., 2014. On the design of exact penalty functions for mpc using mixed integer programming. Computers & Chemical Engineering 70, 104–113.

Johansen, J., Vatland, A., Dec. 5 2000. Method and calcining furnace for electric calcining of carbonaceous material. US Patent 6,157,667.

King, J., Please, C., Hagan, P., 1990. Anthracite carbonizer.

Kosowska-Golachowska, M., Gajewski, W., Musiał, T., 2014. Determination of the effective thermal conductivity of solid fuels by the laser flash method. Archives of Thermodynamics 35 (3), 3–16.

Lakomskii, V., Pal'ti, A., Yurchenko, D., 2011. Computer modelling of thermal and electric processes in an electric calcinator. No. 2 Volume 9 2011, 101.

Maciejowski, J. M., 2002. Predictive control: with constraints. Pearson education.

Mayne, D. Q., Rawlings, J. B., Rao, C. V., Scokaert, P. O., 2000. Constrained model predictive control: Stability and optimality. Automatica 36 (6), 789–814.

Meisingset, H. C., 1995. Modelling and model based control of rotary hearth calciner. Ph.D. thesis, NTNU.

Moore, H., 2014. MATLAB for Engineers. Prentice Hall Press.

Murty, H., Biederman, D., Heintz, E., 1969. Kinetics of graphitization-i. activation energies. Carbon 7 (6), 667–681.

Perron, J., Bouvette, J.-F., Dupuis, M., 1996. Optimization of anthracite calcination process in a vertical electric arc furnace. LIGHT METALS-WARRENDALE-, 597–602.

Ritchie, D. M., Kernighan, B. W., Lesk, M. E., 1988. The C programming language. Prentice Hall Englewood Cliffs.

Sælid, S., 1984. Forelesningsnotater i modellering av dynamiske prosesser. Tech. rep., Technical Report 84-2-X, Division of Engineering Cybernetics, NTH, Norway.(in Norwegian).

Savitzky, A., Golay, M. J., 1964. Smoothing and differentiation of data by simplified least squares procedures. Analytical chemistry 36 (8), 1627–1639.

Smalc, M., Shives, G., Chen, G., Guggari, S., Norley, J., Reynolds, R. A., 2005. Thermal performance of natural graphite heat spreaders. In: ASME 2005 Pacific Rim Technical Conference and Exhibition on Integration and Packaging of MEMS, NEMS, and Electronic Systems collocated with the ASME 2005 Heat Transfer Summer Conference. American Society of Mechanical Engineers, pp. 79–89.

Speight, J. G., 2005. Handbook of coal analysis. John Wiley & Sons.

Wallouch, R., Fair, F., 1980. Kinetics of the coke shrinkage process during calcination. Carbon 18 (2), 147–153.

Warren, B., 1941. X-ray diffraction in random layer lattices. Physical Review 59 (9), 693.

Wilson, Ø., 2016. Mathematical model of a calcination furnace, specialization project report, Department of Engineering Cybernetics, NTNU.

Yao-jian, R., Zhi, S., Jie, T., Wei, L., 2009. Study on electrolytic aluminium carbon anode preparation with calcined anthracite. Procedia Earth and Planetary Science 1 (1), 694–700.

Appendix A

Numerical values

The numerical values used in the final version of the model is presented in this chapter.

There are three types of values needed for the model: parameters, constants and initial values. The distinction between parameters and constants used here, is that constant are assumed known and unchanging, while the parameters can be estimated to find the curve that best fits the measurements. The initial values gives the start values of the states.

All numerical values for the parameters as well as how they where found are listed in Table A.1. If the found column says "Elkem", it means that Elkem has provided the values. If it says "Guessed" it means that the values are uncertain, and there has been an educated guess while choosing the value. "Estimated" means that the value that gives the best match between the model and the measurements has been estimated, when the other values was fixed.

Table A.1: Parameters values used in the model

Parameter	Symbol	Unit	Value	Found
Reaction rate constant	k_r	$\mathrm{kg/s}$	0.0100446	Estimated
Activation energy	E	$\mathrm{J/mol}$	103978.21	Estimated
Heat capacity of anthracite	C_p	$\mathrm{kJ/(kg\,K)}$	1.26	[1]
Reaction enthalpy of graphitization	ΔH_R	$\mathrm{kJ/kg}$	0	Guessed
Weight fraction of volatiles	X_γ	$-$	0.05	Elkem
Weight fraction of water	$X_{\mathrm{H_2O}}$	$-$	0.08	Elkem
Resistivity of in-feed	ρ_{in}	$\mathrm{m\Omega\,m}$	0.8	Estimated
Thermal conductivity anthracite	k	$\mathrm{kW/(m\,K)}$	0.003	[2]
Emissivity of anthracite	ϵ	$-$	0.95	[3]
Temperature of bottom electrode	$T_{el,b}$	K	2000	Guessed
Temperature of top electrode	$T_{el,t}$	K	2000	Guessed

[1] Engineering Toolbox (2016b)
[2] Kosowska-Golachowska et al. (2014)
[3] Fletcher et al. (1988)

Thermal conductivity of graphite	k_{el}	$\mathrm{kW/(m\,K)}$	0.47	[4]
Resistance factor	k_R	$-$	100	Estimated
Void fraction in volume 1	ν_1	$-$	0.5	Guessed
Void fraction in volume 2	ν_2	$-$	0.4	Guessed
Void fraction in volume 3	ν_3	$-$	0.3	Guessed
Void fraction in volume 4	ν_4	$-$	0.2	Guessed
Void fraction in volume 5	ν_5	$-$	0.1	Guessed
Void fraction in volume 6	ν_6	$-$	0.5	Guessed
Void fraction in volume 7	ν_7	$-$	0.4	Guessed
Void fraction in volume 8	ν_8	$-$	0.3	Guessed
Void fraction in volume 9	ν_9	$-$	0.2	Guessed
Void fraction in volume 10	ν_{10}	$-$	0.1	Guessed
Void fraction in volume 11	ν_{11}	$-$	0.25	Guessed
Void fraction in volume 12	ν_{12}	$-$	0.1	Guessed
Convection coefficient to the wall	h_{wall}	$\mathrm{kW/(m^2\,K)}$	0.2	Guessed
Resistivity of void	ρ_ν	$\mathrm{m\Omega\,m}$	1	Guessed
Resistance loss	R_{loss}	$\mathrm{m\Omega}$	0.531923	Estimated

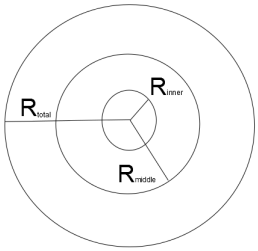

Figure A.1: Furnace radii seen from above

The constants used are listed in Table A.2. The radii are as shown in Figure A.1, and can be chosen such that the size of the control volumes gets desirable. The furnace dimension is confidential, meaning that all values concerning the furnace dimension in any way is marked as such.

Table A.2: Constant values used in the model

Constant	Symbol	Unit	Value	Found
Enthalpy of driving off volatiles	ΔH_{R_γ}	$\mathrm{kJ/kg}$	500	[5]
Enthalpy of vaporizing water	$\Delta H_{R_{\mathrm{H_2O}}}$	$\mathrm{kJ/kg}$	2257	[6]
HHV of methan	$\Delta H_{\mathrm{CH_4,HHV}}$	$\mathrm{kJ/kg}$	55500	[7]

[4] Smalc et al. (2005)
[5] Aylward and Findlay (2008)
[6] Engineering Toolbox (2016a)
[7] Bossel (2003)

Furnace radius	r_{total}	m	Confidential	Elkem
Radius of middle volumes	r_{middle}	m	Confidential	Chosen $< r_{total}$
Radius of inner volumes	r_{inner}	m	Confidential	Chosen $< r_{middle}$
Cross section area of outer volumes	A_{outer}	m^2	Confidential	Calculated
Cross section area of middle volumes	A_{middle}	m^2	Confidential	Calculated
Cross section area of inner volumes	A_{inner}	m^2	Confidential	Calculated
Height of volume 1	z_1	m	Confidential	Chosen
Height of volume 2	z_2	m	Confidential	Chosen
Height of volume 3	z_3	m	Confidential	Chosen
Height of volume 4	z_4	m	Confidential	Chosen
Height of volume 5	z_5	m	Confidential	Chosen
Height of volume 6	z_6	m	Confidential	$= z_1$
Height of volume 7	z_7	m	Confidential	$= z_2$
Height of volume 8	z_8	m	Confidential	$= z_3$
Height of volume 9	z_9	m	Confidential	$= z_4$
Height of volume 10	z_{10}	m	Confidential	$= z_5$
Height of volume 11	z_{11}	m	Confidential	$= z_2$
Height of volume 12	z_{12}	m	Confidential	$= z_3$
Outer cross section area in x-direction 1	A_1	m^2	Confidential	Calculated
Outer cross section area in x-direction 2	A_2	m^2	Confidential	Calculated
Outer cross section area in x-direction 3	A_3	m^2	Confidential	Calculated
Outer cross section area in x-direction 4	A_4	m^2	Confidential	Calculated
Outer cross section area in x-direction 5	A_5	m^2	Confidential	Calculated
Outer cross section area in x-direction 6	A_6	m^2	Confidential	Calculated
Outer cross section area in x-direction 7	A_7	m^2	Confidential	Calculated
Outer cross section area in x-direction 8	A_8	m^2	Confidential	Calculated
Outer cross section area in x-direction 9	A_9	m^2	Confidential	Calculated
Outer cross section area in x-direction 10	A_{10}	m^2	Confidential	Calculated
Outer cross section area in x-direction 11	A_{11}	m^2	Confidential	Calculated
Outer cross section area in x-direction 12	A_{12}	m^2	Confidential	Calculated
Length from middle of volume 1 to border	x_1	m	Confidential	Calculated
Length from middle of volume 2 to border	x_2	m	Confidential	$= x_1$
Length from middle of volume 3 to border	x_3	m	Confidential	$= x_1$
Length from middle of volume 4 to border	x_4	m	Confidential	$= x_1$
Length from middle of volume 5 to border	x_5	m	Confidential	$= x_1$
Length from middle of volume 6 to border	x_6	m	Confidential	Calculated
Length from middle of volume 7 to border	x_7	m	Confidential	$= x_2$
Length from middle of volume 8 to border	x_8	m	Confidential	$= x_2$
Length from middle of volume 9 to border	x_9	m	Confidential	$= x_2$
Length from middle of volume 10 to border	x_{10}	m	Confidential	$= x_2$
Length from middle of volume 11 to border	x_{11}	m	Confidential	Calculated
Length from middle of volume 12 to border	x_{12}	m	Confidential	$= x_{11}$
Thermal conductivity of lining	k_l	$\mathrm{kW}/(\mathrm{m\,K})$	0.0033	Elkem
Thermal conductivity of bricks	k_b	$\mathrm{kW}/(\mathrm{m\,K})$	0.00032	Elkem
Thermal conductivity of steel shell	k_s	$\mathrm{kW}/(\mathrm{m\,K})$	0.052	Elkem

Convection coefficient from steel shell to air	h_{shell}	$\mathrm{kW/(m^2\,K)}$	0.01	Elkem
Width of lining	L_l	m	Confidential	Elkem
Width of bricks	L_b	m	Confidential	Elkem
Width of steel shell	L_s	m	Confidential	Elkem
Temperature of the surrounding	T_0	K	300	Guessed
Radius of top electrode	$r_{el,t}$	m	Confidential	Elkem
Radius of top part of bottom electrode	$r_{el,bt}$	m	Confidential	Elkem
Radius of bottom part of bottom electrode	$r_{el,bb}$	m	Confidential	Elkem
Surface area of top electrode	$A_{el,t}$	$\mathrm{m^2}$	Confidential	Calculated
Surface area of top part of bottom	$A_{el,bt}$	$\mathrm{m^2}$	Confidential	Calculated
Surface area of bottom part of bottom	$A_{el,bb}$	$\mathrm{m^2}$	Confidential	Calculated

The intial values are found in Table A.3. The initial density are used to calculate the initial mass with

$$m_i = \rho_{d,i} V_i \tag{A.1}$$

Table A.3: Initial values used in the model

Initial value	Symbol	Unit	Value	Found
Density in volume 1	$\rho_{d,1}$	$\mathrm{kg/m^3}$	850	Elkem
Density in volume 2	$\rho_{d,2}$	$\mathrm{kg/m^3}$	900	Estimated
Density in volume 3	$\rho_{d,3}$	$\mathrm{kg/m^3}$	950	Estimated
Density in volume 4	$\rho_{d,4}$	$\mathrm{kg/m^3}$	1000	Estimated
Density in volume 5	$\rho_{d,5}$	$\mathrm{kg/m^3}$	1050	Estimated
Density in volume 6	$\rho_{d,6}$	$\mathrm{kg/m^3}$	850	Elkem
Density in volume 7	$\rho_{d,7}$	$\mathrm{kg/m^3}$	900	Estimated
Density in volume 8	$\rho_{d,8}$	$\mathrm{kg/m^3}$	950	Estimated
Density in volume 9	$\rho_{d,9}$	$\mathrm{kg/m^3}$	1000	Estimated
Density in volume 10	$\rho_{d,10}$	$\mathrm{kg/m^3}$	1050	Estimated
Density in volume 11	$\rho_{d,11}$	$\mathrm{kg/m^3}$	1000	Estimated
Density in volume 12	$\rho_{d,12}$	$\mathrm{kg/m^3}$	1050	Estimated
Temperature in volume 1	T_1	K	1590	Estimated
Temperature in volume 2	T_2	K	2045	Estimated
Temperature in volume 3	T_3	K	2150	Estimated
Temperature in volume 4	T_4	K	2080	Estimated
Temperature in volume 5	T_5	K	2000	Estimated
Temperature in volume 6	T_6	K	1600	Estimated
Temperature in volume 7	T_7	K	2100	Estimated
Temperature in volume 8	T_8	K	2200	Estimated
Temperature in volume 9	T_9	K	2100	Estimated
Temperature in volume 10	T_{10}	K	2050	Estimated
Temperature in volume 11	T_{11}	K	2600	Estimated
Temperature in volume 12	T_{12}	K	2700	Estimated

Resistivity in volume 1	ρ_1	$\mathrm{m\Omega\,m}$	0.8	Estimated
Resistivity in volume 2	ρ_2	$\mathrm{m\Omega\,m}$	0.8	Estimated
Resistivity in volume 3	ρ_3	$\mathrm{m\Omega\,m}$	0.8	Estimated
Resistivity in volume 4	ρ_4	$\mathrm{m\Omega\,m}$	0.8	Estimated
Resistivity in volume 5	ρ_5	$\mathrm{m\Omega\,m}$	0.8	Estimated
Resistivity in volume 6	ρ_6	$\mathrm{m\Omega\,m}$	0.8	Estimated
Resistivity in volume 7	ρ_7	$\mathrm{m\Omega\,m}$	0.8	Estimated
Resistivity in volume 8	ρ_8	$\mathrm{m\Omega\,m}$	0.8	Estimated
Resistivity in volume 9	ρ_9	$\mathrm{m\Omega\,m}$	0.7	Estimated
Resistivity in volume 10	ρ_{10}	$\mathrm{m\Omega\,m}$	0.7	Estimated
Resistivity in volume 11	ρ_{11}	$\mathrm{m\Omega\,m}$	0.6	Estimated
Resistivity in volume 12	ρ_{12}	$\mathrm{m\Omega\,m}$	0.35	Estimated